ELECTROMAGNETIC IP RESPONSE OF A CONDUCTING DIKE IN A CONDUCTING EARTH

by

ROBERT ANTHONY CHARTERS
B.Sc., University of Victoria, 1982

A THESIS SUBMITTED IN PARTIAL FULFILLMENT
OF THE REQUIREMENTS FOR THE DEGREE OF
MASTER OF SCIENCE
in the Department
of
Physics

We accept this thesis as conforming
to the required standard

[redacted]

H. W. Dosso M. E. Best

[redacted]

R. M. Clements T. W. Dingle

[redacted]

G. R. Branton

ROBERT ANTHONY CHARTERS
UNIVERSITY OF VICTORIA
August, 1984

Supervisors: Dr. H. W. Dosso and Dr. M. E. Best

ABSTRACT

In this thesis, the electromagnetic coupling component of the spectral IP signal is studied for the case of a vertical conducting dike embedded in a uniform conducting earth. A scale laboratory analogue model was used to obtain spectral IP measurements that were comprised mainly of an electromagnetic coupling component. A graphite plate simulated the dike while a brine solution in a plywood tank simulated the uniform earth. The IP effect for the materials and frequencies used in this model was negligible. Normalized spectral IP measurements were obtained along traverses over the model. These measurements displayed a "gull-wing" anomaly that was symmetrical about the dike. This "gull-wing" feature is typical of the electromagnetic response of a naturally occurring dike. The normalized spectral IP measurements were converted to apparent resistivities that were characteristic of both the dike and the uniform host earth.

Inversions were made of the analogue model apparent resistivities using the Marquardt inversion algorithm and various empirical models of EM coupling based on the Cole-Cole dispersion. The Cole-Cole dispersion is not a suitable model

for EM coupling since it yields only apparent resistivities with small, negative phases. The phase of the analogue model apparent resistivity in the region over the dike is positive. Inversions of analogue model apparent resistivities were made using the generalized Cole-Cole dispersion and the product of two generalized Cole-Cole dispersions. The inversion calculations broke down in the region of positive phase over the dike, but successful inversions were made in regions far from the dike. It was concluded, therefore, that the Cole-Cole dispersion and its derivatives were better suited to modeling EM coupling for a uniform earth than for a conducting body embedded in a uniform host earth.

An analytical model of EM coupling for the embedded dike was developed, and is referred to as the Dipole-Dipole-Loop (DDL) model. In the DDL model, the dike embedded in a uniform host earth was replaced by a conducting loop embedded in a uniform half-space. The resulting EM coupling was derived using the principles of electromagnetic induction. All linear current elements in the DDL model were treated as strings of point electric dipoles. The expressions for the EM fields of a point electric dipole embedded in, or on the surface of, a uniform conducting half-space are well known.

The analogue model apparent resistivities were inverted using the DDL model. Inversions were made of apparent resis-

tivities along individual traverses for different frequencies and dipole separations with the dike at a constant depth. Excellent agreement was obtained between the DDL model and analogue model apparent resistivities along these traverses. The parameters of the DDL model were constant with array position, but varied with frequency and dipole separation, indicating that an equivalent current loop existed for each electromagnetic configuration of the conducting dike. Thus, the DDL model was capable of describing EM coupling for the embedded dike for the whole frequency range of measurements obtained. Further work is required before the frequency dependence of the DDL model parameters for the embedded dike can be predicted. When this is achieved, the DDL model will provide more accurate descriptions of EM coupling for buried ore bodies and will facilitate removal of the EM coupling component from the spectral IP signal obtained from such bodies.

[redacted]

H. W. Dosso M. E. Best

[redacted]

R. M. Clements T. W. Dingle

[redacted]

G. R. Branton

ELECTROMAGNETIC IP RESPONSE OF A CONDUCTING DIKE IN A CONDUCTING EARTH

TABLE OF CONTENTS

Page

Page

LIST OF FIGURES

FIGURE Page

FIGURE Page

ACKNOWLEDGEMENTS

I would like to thank my supervisors, Dr. H. W. Dosso and Dr. M. E. Best for their valuable guidance throughout the research.

I would also like to thank Dr. J. T. Weaver, Dr. W. Neinaber, Dr. G. Heard, Mr. W. Hu, of the University of Victoria, and the geophysicists of the mineral exploration staff at Shell Canada Resources Limited for many useful discussions and comments.

Financial support for this work was in part provided by Shell Canada Resources Limited of Calgary, Alberta. The financial support of N.S.E.R.C. scholarships is gratefully acknowledged.

CHAPTER I

INTRODUCTION

1.1 The Problem

Over the last two decades, the induced polarization (IP) technique has received increased attention from exploration geophysicists in mineral ore exploration, and, more recently, in oil and natural gas exploration. The IP survey offers two major advantages over other commonly used exploration techniques. Firstly, it is a controlled source survey. An electrical current of known strength is injected into the earth at a transmitter that is normally connected to the ground at two points (a dipole). The electrical response of the earth is measured as an induced potential across a dipole receiver. Since the characteristics of the input current and the measured potential are both known, the transfer impedance of the earth can be calculated without undue difficulty. Secondly, the equipment used in an IP survey is small and portable, making the survey relatively inexpensive to conduct. This is particularly attractive to petroleum exploration geophysicists who, at present, depend mostly on expensive seismic surveys.

The primary characteristic of the earth measured in an IP survey is the earth's ability to store electrical energy as an accumulation of electrical charge, or polarization, that is induced by the potential of the transmitter. This ability varies with the physical and chemical nature of the region of the earth being explored. Consequently, IP measurements provide a means by which the composition of underlying formations might be deduced.

There are two techniques for IP surveys: the time domain IP technique and the frequency domain (spectral) IP technique. In the time domain IP technique a direct current is injected through the transmitter dipole. In the spectral IP technique, a sinusoidal alternating current is injected through the transmitter dipole. The spectral IP technique allows measurements to be made over a spectrum of different frequencies of transmitter current and is the technique currently receiving the most attention in the literature.

In both mineral and petroleum exploration, the discovery of large, shallow ore bodies and petroleum reservoirs is becoming increasingly rare. Exploration geophysicists have been forced to look for smaller and deeper deposits. This requires increased resolution and depth of penetration in the probing signal. In the spectral IP technique, this is achieved by increasing the transmitter frequency and lengthing the separation distance between the transmitter and the receiver dipoles

(dipole separation). Unfortunately, when large frequencies and large dipole separations are used over terrains with relatively high conductivities, such as sedimentary basins, the electromagnetic (EM) responses from capacitive coupling between the transmitter and receiver cable, and EM coupling between the dipole array and the conducting earth, can become such large components of the total measured response (the spectral IP signal) that they completely mask the IP component.

Under these conditions, it is necessary to isolate and remove the EM coupling component from the spectral IP signal to facilitate more accurate interpretation of the IP component. In order to achieve this separation, it is necessary to study the nature of EM coupling and find a means of quantifying its electromagnetic response. This is the problem to which this thesis is addressed.

1.2 The Spectral Induced Polarization Technique

The important elements of the spectral IP technique are illustrated in Fig. 1. Each of the receiver and transmitter consists of a pair of grounded electrodes which are electrically connected at the surface by a shielded cable. An alternating sinusoidal current of fixed amplitude is injected

SPECTRAL INDUCED POLARIZATION SURVEY

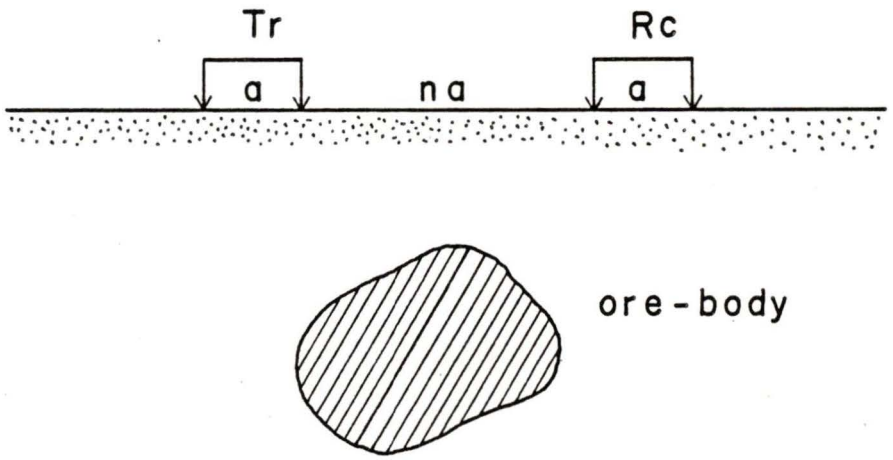

Array In-Line Dipole-Dipole

a = dipole length

na = dipole separation n=1,2,3,4

Frequency Range .25 Hz - 512. Hz

Apparent Resistivity $\rho_a = \pi n(n+1)(n+2)a\frac{V}{I}$

Fig. 1 Elements of a Spectral Induced Polarization Survey

through the transmitter dipole. The earth's electromagnetic response to this current is then measured as a phase-delayed sinusoidal potential across the receiver dipole. The phase of this potential is measured with respect to the transmitter current.

In a typical spectral IP survey, each of the transmitter and receiver dipoles is arranged with the two contacts of the dipole along the survey axis. The lengths of the transmitter and receiver dipoles are equal and have values, 'a', that vary from 10 m to 1000 m. The dipole separation is equal to an integral number of dipole lengths. Such a configuration is referred to as an in-line dipole-dipole array. As a rule of thumb, the maximum depth of penetration of the probing signal is approximately one-half the dipole separation.

In a spectral IP survey, measurements are made over a grid of traverses covering a region of the earth suspected of containing minerals which cause an IP effect. Each traverse consists of a number of measuring stations along the axis of the traverse. At each station, a complex potential is measured for a number of discrete transmitter frequencies in the range of .01 Hz to 1000 Hz, and for dipole separations 'na' (n = 1, 2 --- 6), where 'a' is the dipole length. Thus, at each station, a spectrum of complex potentials is measured for each

dipole separation.

It is customary to convert each complex potential into an apparent resistivity. The mathematical expression used for this conversion depends on the geometry of the probing array. The apparent resistivity expression for an in-line dipole-dipole array is (Sumner, 1976)

$$\rho_a = \pi n (n+1)(n+2) a \frac{V}{I} \quad , \qquad (1.1)$$

where ρ_a is the apparent resistivity (Ω-m), a is the dipole length (m), n is the dipole separation integer, V is the measured complex potential (volts), and I is the transmitter current (amperes). Since (1.1) involves the ratio $\frac{V}{I}$, the apparent resistivity is proportional to the transfer impedance of the earth. Apparent resistivities from spectral IP surveys are typically presented in a pseudo-section format as shown in Fig. 2. The horizontal axis is station position along a traverse, and the vertical axis is dipole separation, representing the approximate depth of penetration. A resistivity amplitude and phase are assigned to each point on the graph and the values are contoured. The contours are used to interpret the conductivity structure of the region being probed.

1.3 The Spectral Induced Polarization Signal

The signal measured in a spectral IP survey is a compo-

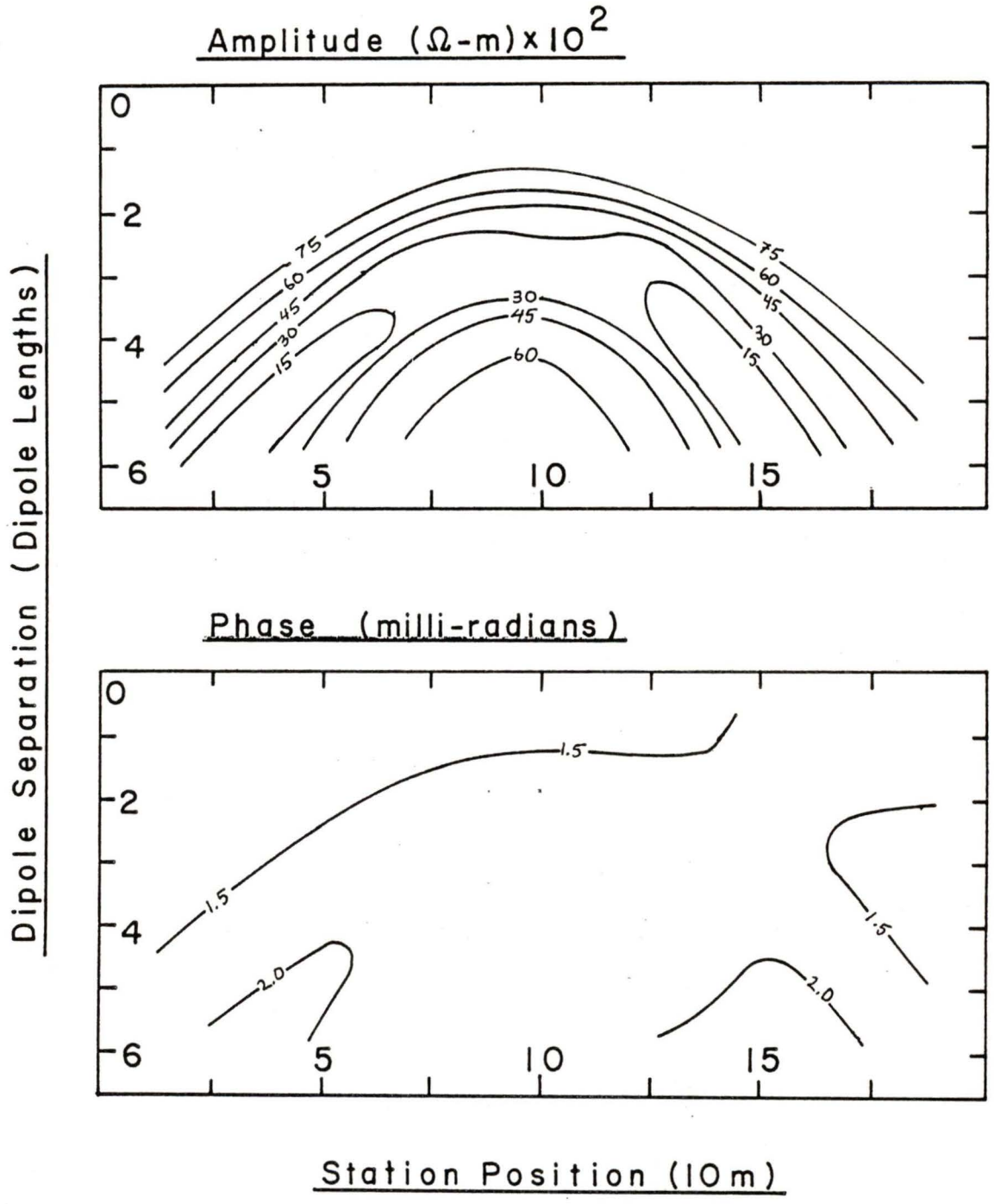

Fig. 2 A Typical Apparent Resistivity Pseudo-Section of a Dike-like Ore Body in New Brunswick (Compliments of Shell Canada Resources Ltd.)

site of electrical responses from the earth and from the dipole array itself. Three of the more important responses are IP and EM induction, each of which is an earth response, and capacitive coupling, which is an array response. Presented here is a brief descriptive review of each of these effects. A detailed analysis of the physical and chemical basis of IP is given by Zonge (1972). Wynn (1974) presents a detailed analysis of EM induction and capacitive coupling.

(i) Induced Polarization

IP arises from the accumulation of electrical charge at various electrical interfaces in the earth. These accumulations occur independently of any displacement currents that are induced. In fact, at the low frequencies used in spectral IP surveys, the contribution from displacement currents is negligible (Zonge, 1972). Instead, most of the IP effect arises from interaction between electrolytic pore fluids and their surrounding host rocks. It has been well demonstrated that dry rocks display a negligible IP effect, whereas the maximum response is measured from porous rocks saturated with an electrolytic pore fluid.

Zonge (1972) classified the IP effect in two major categories: electrode polarization and membrane polarization.

Electrode polarization arises when current flows through an electrochemical system consisting of electrodes (metallic mineral particles) and electrolyte (pore fluids). Such a system is illustrated in Fig. 3(a) by a metallic particle blocking an electrolyte-filled pore. The two metal-electrolyte interfaces of the particle behave like a coupled electrode pair. When a potential is established across the metallic particle, two types of current are induced: Faradaic and non-Faradaic.

Faradaic current results from charge transfer reactions that occur at the electrode interface. The rate of charge transfer from the ions in the electrolyte to the metallic particle depends largely on the oxidation-reduction properties of the ions in solution, and on the rate at which ions are made available for oxidation or reduction at the interface. Zonge (1972) has determined that the rate of reaction is governed primarily by the diffusion speed of the ions in solution. He called the system mass transfer limited. Since the speed of charge transfer at the electrode is greater than the rate of mass transfer, a depletion of ions of a given polarization occurs at one interface while an accumulation occurs at the other interface.

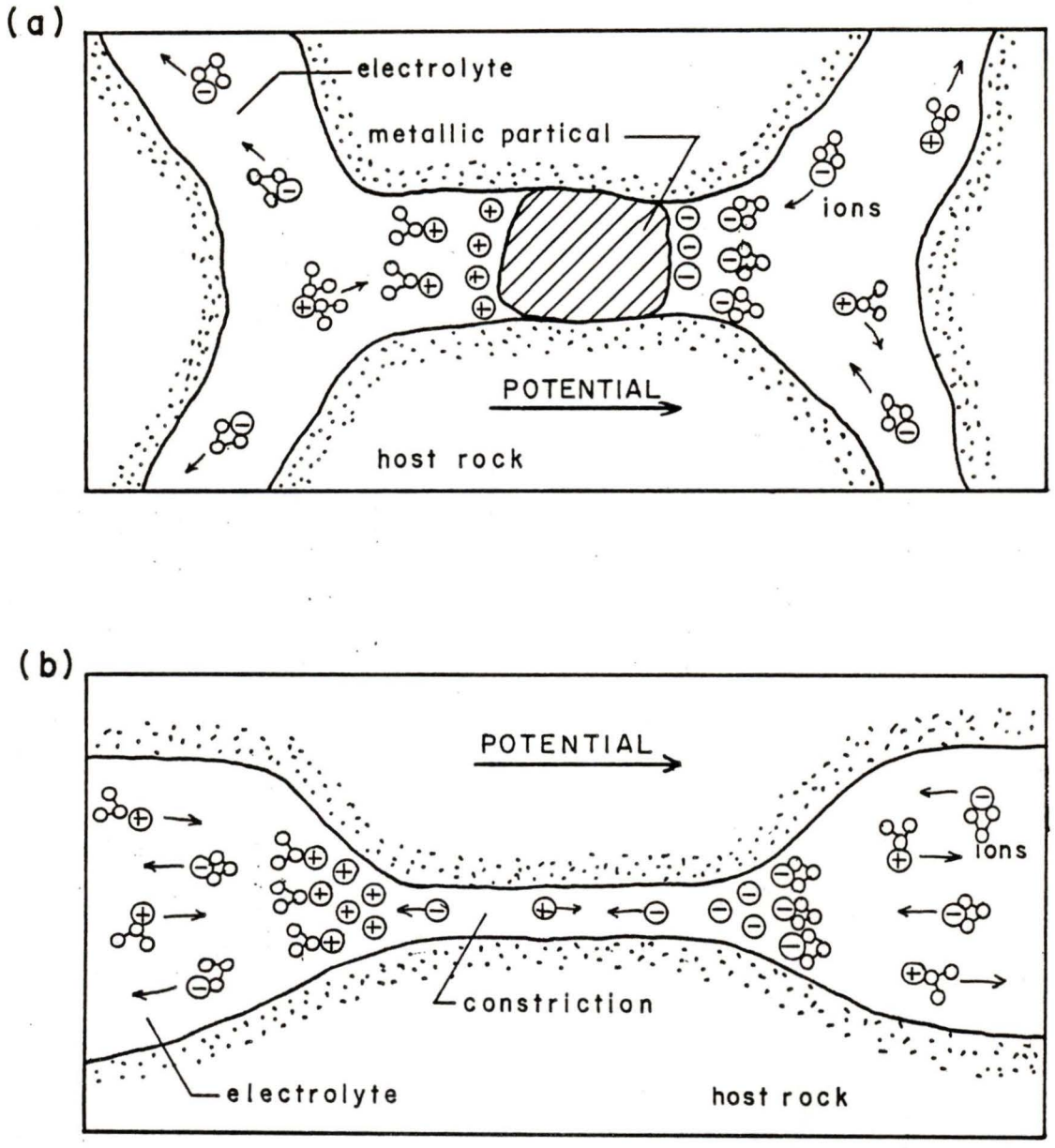

Fig. 3 Mechanisms of the IP Effect
(a) Electrode Polarization
(b) Membrane Polarization

Non-Faradaic current arises when the ions in solution cannot be oxidized or reduced under the prevailing potentials. When the metallic particle is polarized by a potential, it attracts ions of the opposite polarity. These ions accumulate at the electrode interface and establish the so-called double layer. The layer nearest to the electrode consists of densely packed non-hydrated ions. The next layer consists of closely packed hydrated ions. Outside this layer is a diffuse layer of hydrated ions of the same polarity as those in the inner layers. When the potential across the electrode changes from equilibrium, the charges in the double layer redistribute themselves causing a diffusion current to flow until a new equilibrium is reached. The double layers at opposite interfaces of the metallic particle have opposite polarity. Thus, the electrode polarization is the net result of Faradaic and double-layer current flow at the electrode interfaces.

It has often been observed that rocks containing apparently no metallic mineral content also display an IP effect. This is due to membrane polarization which occurs where deformations in the host rock constrict the cross sectional area of electrolyte-filled pores as illustrated in Fig. 3(b). Normally, many water molecules are adsorbed to the sides of the pores, further constricting the cross sectional area. Ions

flowing through this restricted space will experience an increase in viscosity due to van der Waal's forces exerted by the water molecules adsorbed to the pore sides. This decreases the mobility of the ions in the restricted space, effectively increasing the electrical resistivity with respect to ionic currents. Consequently, ions of a given polarity will accumulate on one side of the constriction and be depleted on the opposite side. Since ions of opposite polarity flow in opposite directions in response to the impressed potentials, charges of opposite polarity will accumulate on opposite sides of the constriction.

In a spectral IP survey the transmitter radiates sinusoidally varying inducing fields. The charging and discharging of electrode and membrance polarizations are expressed as a phase delay in the sinusoidal potential registered at the receiver.

The ability of the earth to store electrical energy as induced polarization was first observed by Schlumberger (1920). Schlumberger patented some of his ideas on IP in 1912. He observed that samples of metallic ores tended to store electrical charge when a direct current was passed through them. The rate of electrical discharge, when the current was switched off, seemed to depend on the mineral composition of the sample (Schlumberger, 1920). He concluded erroneously that the IP

effect was limited to metallic minerals. He soon found, however, that his measurements in the field were being contaminated by non-metallic based electromagnetic noise that tended to mask the response from metallic ores. This led him to abandon the technique. Schlumberger's negative results tended to discourage significant research in IP for another two decades.

It was not until Brant (1946) and his research associates at Newmont Exploration Limited rediscovered the IP effect, that further advances were made. Brant was one of the first to recognize the non-metallic origins of the IP effect. The research performed at Newmont is well summarized in a set of papers edited by Wait (1959) entitled, "Over Voltage Research and Geophysical Application". Brant's work sparked a number of IP effect investigations. Bleil (1953) published a review of applications, and Madden and Marshall (1958, 1959a, 1959b) researched the electro-thermodynamic nature of IP. Other major contributors to IP research were Siegal (1959) who developed a mathematical formulation of IP based on chargeabilities, Hallof (1965) who developed a method of interpreting spectral IP phase measurements, Zonge (1972) who developed a number of equivalent circuit representations of IP, and Pelton (1977) who developed the Cole-Cole dispersion representation of apparent resistivity spectra for the IP effect.

Comprehensive reviews of IP are given by Madden (1967) and Sumner (1976). Sumner (1976) also provides an extensive history of previous IP research, with complete references.

(ii) Electromagnetic Induction

The second major component of the spectral IP signal results from EM induction, the main topic of this thesis. The EM component is less complex in nature than the IP component. EM induction arises when the EM fields from the transmitter induce electrical eddy currents in conducting regions of the earth. These eddy currents then radiate EM fields which are registered at the receiver as a phase delayed potential. The total potential due to EM induction registered at the receiver consists of the primary potential due to EM fields that propagate in the earth directly from the transmitter, and the secondary potential due to fields that propagate from the induced eddy currents in the earth. That component of the spectral IP signal resulting from EM induction is referred to as EM coupling, the receiver and transmitter being electromagnetically coupled to the region of the earth under study.

Examples of conducting regions in the earth are mineral ore bodies, such as intrusive dikes and sills with high concentrations of metals or graphite, and porous rocks that have

high fluid permeabilities and are saturated by an electrolytic pore fluid. An example of the latter would be a sandstone or shale charged with fossil sea waters.

In principle, expressions for EM coupling can be derived by the application of local boundary conditions to Maxwell's field equations. In practice, analytical solutions have been obtained for only a few simple geometries. For example, Sunde (1949) developed an analytical expression for the EM coupling between two arbitrarily oriented grounded wires on the surface of a uniform conducting half-space. Millet (1967) applied Sunde's (1949) development to the special case of an in-line dipole-dipole array. Millet (1967) found that for the case of an homogeneous earth, EM coupling increases with increasing earth conductivity, transmitter frequency, dipole length, and dipole separation. Wait (1953), Ness (1963), Dey and Morrison (1973), Hohmann (1973) and Wynn (1974) have calculated the electromagnetic coupling for an in-line dipole-dipole array over a layered earth, and Wynn (1974) and Wait (1984) have developed expressions for EM coupling over an anisotropic earth. In related studies, Baños (1966), Weaver (1967), Hohmann (1974), Ramaswamy (1973, 1978) and Wait (1966, 1970, 1971) have studied the propagation of point electric dipole fields in uniform and layered earths.

Most analytical work to date has focussed on EM coupling over a laterally uniform earth. Some exceptions are Naidu (1966) and Wiedelt (1983) who examined EM coupling over perfectly conductive vertical dikes in a non-conducting host earth. To date, no-one has fully formulated EM coupling for a dipole-dipole array over a conducting earth containing a more conductive body of simple geometry. Wynn's (1974) review provides many useful references on the topic of EM coupling in the spectral IP signal.

(iii) Capacitive Coupling

Capacitive coupling arises when a potential is induced in the receiver from leakage and displacement currents, and mutual inductance between cables linking the transmitting and receiving equipment (Wynn, 1974). Leakage and displacement currents usually result from imperfectly insulated transmitter wires in contact with a wet earth. Mutual inductance results when reference cables linking the transmitter and receiver to the recording device are placed in a parallel configuration too near each other. If the survey is carried out under such non-optimum conditions, the recorded data may be seriously contaminated by the effects of capacitive coupling. However, under well controlled conditions, the effects of capacitive coupling

can be minimized. In most spectral IP surveys capacitive coupling is the least important of the three signal responses and as such, will not be dealt with in this work. It is referred to here only for completeness.

To summarize, the spectral IP signal contains three major components: that due to capacitive coupling and those due to the IP effect and EM coupling. The effect of capacitive coupling can be minimized by improved cable quality and configuration. IP depends principally on the physical and chemical nature of the earth, while the EM coupling effect depends on the gross conductivity structure of the earth. If the IP component and the EM component could be separated, exploration geophysicists could gain information on the target composition using the IP component, and gain information on the target geometry and conductivity structure using the EM coupling component.

1.4 The Removal of the Electromagnetic Coupling Component from the Spectral Induced Polarization Signal

Wynn (1974) summarized the history of techniques for the removal of the EM coupling component from the spectral IP signal. Perhaps the simplest solutions to EM coupling removal were achieved with specialized field techniques. These were

also the most restrictive. It was generally realized that the EM coupling effect becomes important at higher frequencies and larger dipole separations. Consequently, surveys were conducted in which the maximum frequency was limited to 1 Hz and dipole lengths were kept on the order of meters. Unfortunately, valuable information obtainable at frequencies as high as 100 Hz was, therefore lost. In addition, the depth of penetration was limited to a few 10's of meters. In view of these problems, exploration geophysicists tried redesigning the probing array by rotating the receiver dipole by 90° so that it straddled the traverse axis. This array decreased the size of the EM coupling component relative to the IP component. Unfortunately, this reduced the total strength of the recorded spectral IP signal. Thus, these techniques for "avoiding" EM coupling proved to be too restrictive for general use.

Hallof (1973) made use of the fact that EM coupling decreases with decreasing frequency. He measured the phase at a few discrete frequencies and extrapolated the measured values back to 0 Hz (or DC), using a linear or quadratic relationship. He then interpreted these DC values as being the IP response in the absence of EM coupling. This technique was subject to inaccuracies arising from the assumptions made by Hallof (1973) concerning the linear nature of the frequency response of the

phase of the spectral IP signal. These assumptions were not always valid.

Other techniques for removing EM coupling have been based on inverting the field data using numerical models of EM coupling. Though several authors have developed theoretical estimates of EM coupling for various earth geometries, as discussed earlier, few (e.g. Wynn, 1974; Pelton, 1977) have attempted to use numerical models to remove EM coupling by inverting field data. There are several algorithms available for inverting field data; a ridge regression algorithm used by Pelton (1977), and the Marquardt (1963) algorithm, modified by Anderson (1977) are two examples. The Marquardt inversion algorithm will be used in this thesis. In the Marquardt inversion algorithm a function

$$\Phi = \sum_{i=1}^{n} \omega_i \left(Y_i - F_i \left(b_1, b_2 \cdots b_m \right) \right)^2 \qquad (1.2)$$

is calculated. This function is a weighted sum of square errors between the observed data Y_i and the calculated data F_i (function of parameters b_j, $j = 1,m$). Φ is minimized with respect to the parameters b_j, using a combination of Newton's technique and the method of steepest descent. The resulting parameters b_j describe that function F which best fits the observed data in the least squares sense.

Wynn (1974) inverted observed apparent resistivity spectra measured over regions with a negligible IP effect using various layered earth models. Pelton's (1977) approach was to fit the product of two Cole-Cole dispersions to the data: one to describe the IP effect and the other to describe EM coupling. He thus obtained an empirical estimate of EM coupling. This technique will be explored in more depth later in this thesis. One important observation to be made here is that, to the author's knowledge, with the exception of Pelton (1977), attempts have been made to remove only the effects of EM coupling for a laterally uniform earth, and to date, no attempts have been made to remove EM coupling due to finite conductors such as ore bodies.

1.5 The Work Covered in this Thesis

The purpose of the work reported in this thesis was to study the response of EM coupling for the case of a vertical conducting dike embedded in a poorly conducting uniform earth. A laboratory scale analogue model was used to obtain spectral IP measurements along traverses over an embedded dike model. For this graphite dike model, it was assumed that the IP response was negligible and that the model field measurements were primarily due to the EM coupling effect. The laboratory

model measurements were inverted using several different empirical models of EM coupling, namely the Cole-Cole dispersion model and its derivatives.

An analytical model of EM coupling for the case of the conducting dike embedded in a uniform poorly conducting earth is developed. This model is referred to as the dipole-dipole-loop model. Results of inverting the laboratory measurements using the dipole-dipole-loop model are presented. Conclusions are presented on the use of this analytical model in removing the EM coupling component from the spectral IP signal, and recommendations are made concerning further development of numerical models of EM coupling for use in the case of a conducting body in a uniform conducting host earth.

CHAPTER 2

THE LABORATORY ANALOGUE SCALE MODEL

2.1 Analogue Model Scaling Conditions

For the study of EM coupling, the ideal spectral IP measurements would be those in which the IP component is absent or negligible. This is difficult to achieve in the field, since there is always uncertainty about the underlying geology. In addition, coherent and random electromagnetic noise, over which the surveyor has no control, is always present. As a result, it is necessary to turn to laboratory scale models which can be designed to yield spectral IP measurements with the desired character.

A naturally occurring electromagnetic system can be reduced to a laboratory scale model only when certain scaling conditions are met. The theory of electromagnetic scaling has been developed by such authors as Strangeway (1966) and Frischknecht (1971), and has been applied by Dosso (1966a). Presented here is a brief derivation of the scaling conditions used to design the laboratory scale model of a dike in a poorly conducting host earth.

In the following analysis, System International units will be used with conductivities expressed in Siemens per meter $(S\,m^{-1})$.

Let $p'(x', y', z')$ be a point in the naturally occurring (geophysical) system. Let $p(x, y, z)$ be a point in the scale model system. Assume that the transformation of coordinates from the geophysical system to the model system is linear; that is

$$x' = px \quad , \quad y' = py \quad , \quad z' = pz \quad . \tag{2.1}$$

The same unit of length is used in both systems, and all three dimensions scale in the same way.

In linear isotropic media, free of electromagnetic sources, Maxwell's field equations can be written as:

$$\nabla \times \underset{\sim}{E}(x, y, z, t) = -\mu \frac{\partial}{\partial t} \underset{\sim}{H}(x, y, z, t) \quad , \tag{2.2}$$

$$\nabla \times \underset{\sim}{H}(x, y, z, t) = \sigma \underset{\sim}{E}(x, y, z, t) + \epsilon \frac{\partial \underset{\sim}{E}}{\partial t} \quad , \tag{2.3}$$

where $\underset{\sim}{E}$ and $\underset{\sim}{H}$ are the electric and magnetic field intensities respectively, μ and ϵ are the permeability and permittivity of the medium and σ is the conductivity of the medium.

Maxwell's equations are invariant under linear transformation of coordinates. Consequently, $\underset{\sim}{E}$, $\underset{\sim}{H}$ and time t must

transform, at most, linearly, that is

$$\underset{\sim}{E}'(x',y',z',t') = a\,\underset{\sim}{E}(x,y,z,t) \quad , \tag{2.4}$$

$$\underset{\sim}{H}'(x',y',z',t') = b\,\underset{\sim}{H}(x,y,z,t) \quad , \tag{2.5}$$

$$t' = c\,t \quad . \tag{2.6}$$

The primed variables represent the geophysical system, while the unprimed variables represent the scale model system.

In general, the media in which the EM fields are established are inhomogeneous, and the parameters are written as

$$\sigma = \sigma(x,y,z,t) \quad , \tag{2.7}$$

$$\mu = \mu(x,y,z,t) \quad , \tag{2.8}$$

$$\epsilon = \epsilon(x,y,z,t) \quad . \tag{2.9}$$

Consider equation (2.2) in the model system,

$$\nabla \times \underset{\sim}{E} = -\mu \frac{\partial}{\partial t} \underset{\sim}{H} \quad .$$

Transform the right hand side to geophysical coordinates to yield

$$\nabla \times \underset{\sim}{E} = -\mu \frac{\partial \underset{\sim}{H}}{\partial t'} \frac{\partial t'}{\partial t} = -\mu \frac{c}{b} \frac{\partial \underset{\sim}{H}'}{\partial t'} \quad . \tag{2.10}$$

Now consider the left hand side of (2.10);

$$(\nabla \times \underset{\sim}{E})_x = \frac{\partial E_z}{\partial y} - \frac{\partial E_y}{\partial z} = \frac{\partial E_z}{\partial y'}\frac{\partial y'}{\partial y} - \frac{\partial E_y}{\partial z'}\frac{\partial z'}{\partial z} ,$$

$$= \frac{P}{a}\left(\frac{\partial E_z'}{\partial y'} - \frac{\partial E_y'}{\partial z'}\right) ,$$

or

$$(\nabla \times \underset{\sim}{E}) = \frac{P}{a}(\nabla' \times \underset{\sim}{E}') . \qquad (2.11)$$

Combine (2.10) and (2.11) to yield

$$\frac{P}{a}(\nabla' \times \underset{\sim}{E}') = -\mu \frac{c}{b}\frac{\partial}{\partial t'}\underset{\sim}{H}' ,$$

or

$$(\nabla' \times \underset{\sim}{E}') = -\mu \frac{a}{P}\frac{c}{b}\frac{\partial}{\partial t'}\underset{\sim}{H}' . \qquad (2.12)$$

Now consider equation (2.3);

$$(\nabla \times \underset{\sim}{H}) = \sigma \underset{\sim}{E} + \epsilon \frac{\partial \underset{\sim}{E}}{\partial t} = \frac{\sigma}{a}\underset{\sim}{E}' + \epsilon \frac{c}{a}\frac{\partial \underset{\sim}{E}'}{\partial t'} ,$$

and

$$(\nabla \times \underset{\sim}{H}) = \frac{P}{b}(\nabla' \times \underset{\sim}{H}') ,$$

which leads to

$$(\nabla' \times \underset{\sim}{H}') = \sigma \frac{b}{aP}\underset{\sim}{E}' + \epsilon \frac{cb}{Pa}\frac{\partial \underset{\sim}{E}'}{\partial t'} ,$$

$$= \sigma' \underset{\sim}{E}' + \epsilon' \frac{\partial \underset{\sim}{E}'}{\partial t'} . \qquad (2.13)$$

In order for Maxwell's equations to be invariant under the

coordinate transformation, equations (2.12) and (2.13) must be identities. Therefore, equations (2.12) and (2.13) lead to

$$\mu'(x', y', z') = \frac{ca}{pb}\,\mu(x, y, z) \quad , \tag{2.14}$$

$$\sigma'(x', y', z') = \frac{b}{pa}\,\sigma(x, y, z) \quad , \tag{2.15}$$

and

$$\epsilon'(x', y', z') = \frac{bc}{pa}\,\epsilon(x, y, z) \quad . \tag{2.16}$$

In many geophysical problems the permeabilities of the media are not significantly different from that of free space. If the permeabilities in the model materials also have values near the permeability of free space, then it can be assumed that

$$\mu' = \mu = \mu_o \quad ,$$

and

$$\frac{ca}{pb} = 1 \tag{2.17}$$

If it is also reasonable to neglect displacement currents in both the geophysical and model systems, then equation (2.16) can be ignored, leaving equations (2.17) and (2.15). Let

$$\frac{a}{b} = \frac{E'}{E}\cdot\frac{H}{H'} = \left(\frac{E'}{H'}\right)\Big/\left(\frac{E}{H}\right) = \kappa \tag{2.18}$$

where $\mathcal{K}$ is the electromagnetic impedance scale factor.

Using (2.18), equations (2.17) and (2.15) become

$$\frac{c\mathcal{K}}{p} = 1 \quad ,$$

and

$$\sigma' = \frac{\sigma}{p\mathcal{K}} \quad . \tag{2.19}$$

The angular frequency ω is given by $\omega = \frac{2\pi}{T}$, where T is the period of variation. Since $t' = ct$, $T' = cT$, and

$$\omega' = \frac{1}{c}\omega$$

Thus, equations (2.19) become

$$\frac{\omega\mathcal{K}}{p} = \omega' \quad , \tag{2.20}$$

and

$$\frac{\sigma}{p\mathcal{K}} = \sigma' \quad . \tag{2.21}$$

Consider the product of (2.20) and (2.21)

$$\frac{\omega\sigma}{p^2} = \omega'\sigma' \quad ,$$

or

$$p^2 = \left(\frac{\sigma}{\sigma'}\right)\left(\frac{\omega}{\omega'}\right) \quad ,$$

and since P is the scale factor for lengths L and L',

$$\left(\frac{L'}{L}\right)^2 = \left(\frac{\sigma}{\sigma'}\right)\left(\frac{\omega}{\omega'}\right) \quad ,$$

or

$$\left(\frac{\sigma}{\sigma'}\right)\left(\frac{\omega}{\omega'}\right)\left(\frac{L}{L'}\right)^2 = 1 \quad , \tag{2.23}$$

the model scaling condition.

To summarize, a geophysical EM system can be reduced to a laboratory scale model if the following conditions are met:

(a) The permeabilities of the media in both the geophysical and the scale model systems are not significantly different from the permeability of free space.

(b) The permittivities of the media in both the geophysical and scale model systems are not significantly different from the permittivity of free space.

(c) The scale factors used to design the scale model satisfy equation(2.23).

These conditions have been applied in designing the laboratory scale model for the problem of EM coupling in the case of a conducting dike in a poorly conducting uniform host

earth. The restrictions on μ and ϵ have been satisfied by using appropriate materials in the model, while the restriction (2.23) has been satisfied by using appropriate dimensions in the model. These will be described in detail in the following sections.

2.2 The Laboratory Analogue Model Facility

The laboratory analogue model facility used to study the scale model of a conducting dike in a poorly conducting uniform host earth is illustrated in Fig. 4 and Fig. 5. A graphite plate was used to simulate the conducting dike, while a brine-filled tank was used to simulate the poorly conducting host earth. The graphite dike was immersed in the brine vertically at a specified depth, in the central region of the tank. Spectral IP measurements were carried out along traverses over the dike, perpendicular to its strike.

Four copper electrodes, 30 cm long by .5 cm in diameter, were used to simulate the in-line dipole-dipole array. These electrodes were mounted on a lucite carriage drawn by an electric motor along a wooden beam straddling the tank. The end of each electrode just touched the surface of the brine. The leading pair of electrodes formed the receiver dipole, while the trailing pair of electrodes formed the transmitter dipole.

Apparatus

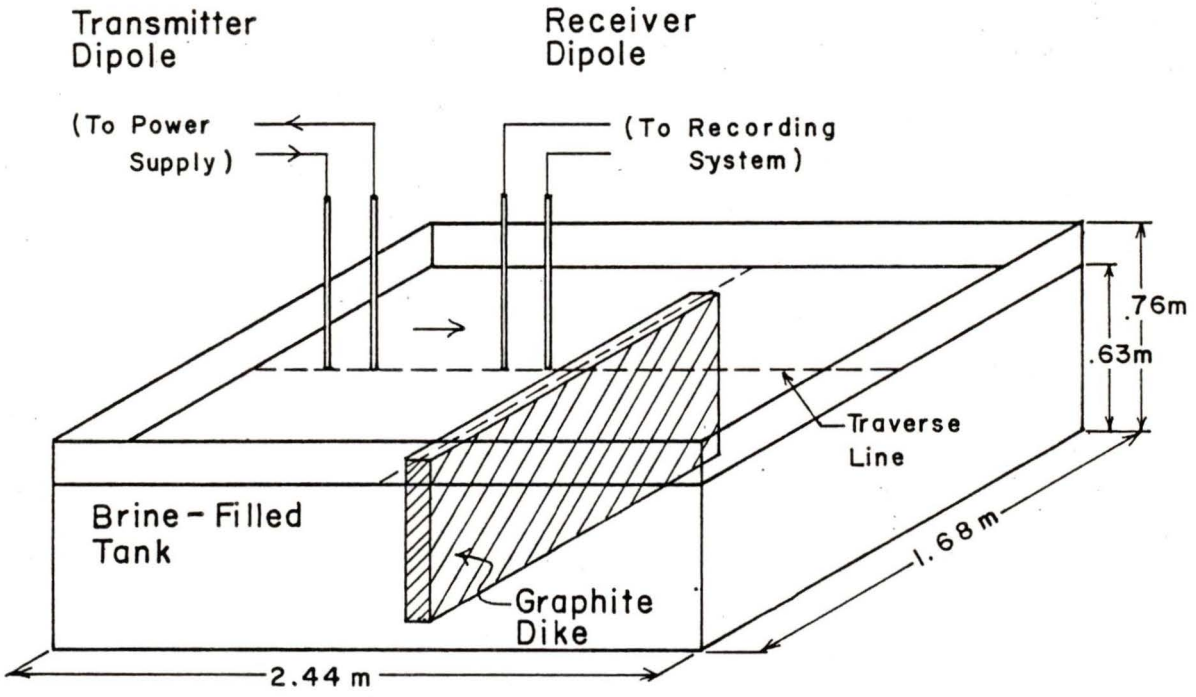

Fig. 4 The Laboratory Analogue Modeling Facility

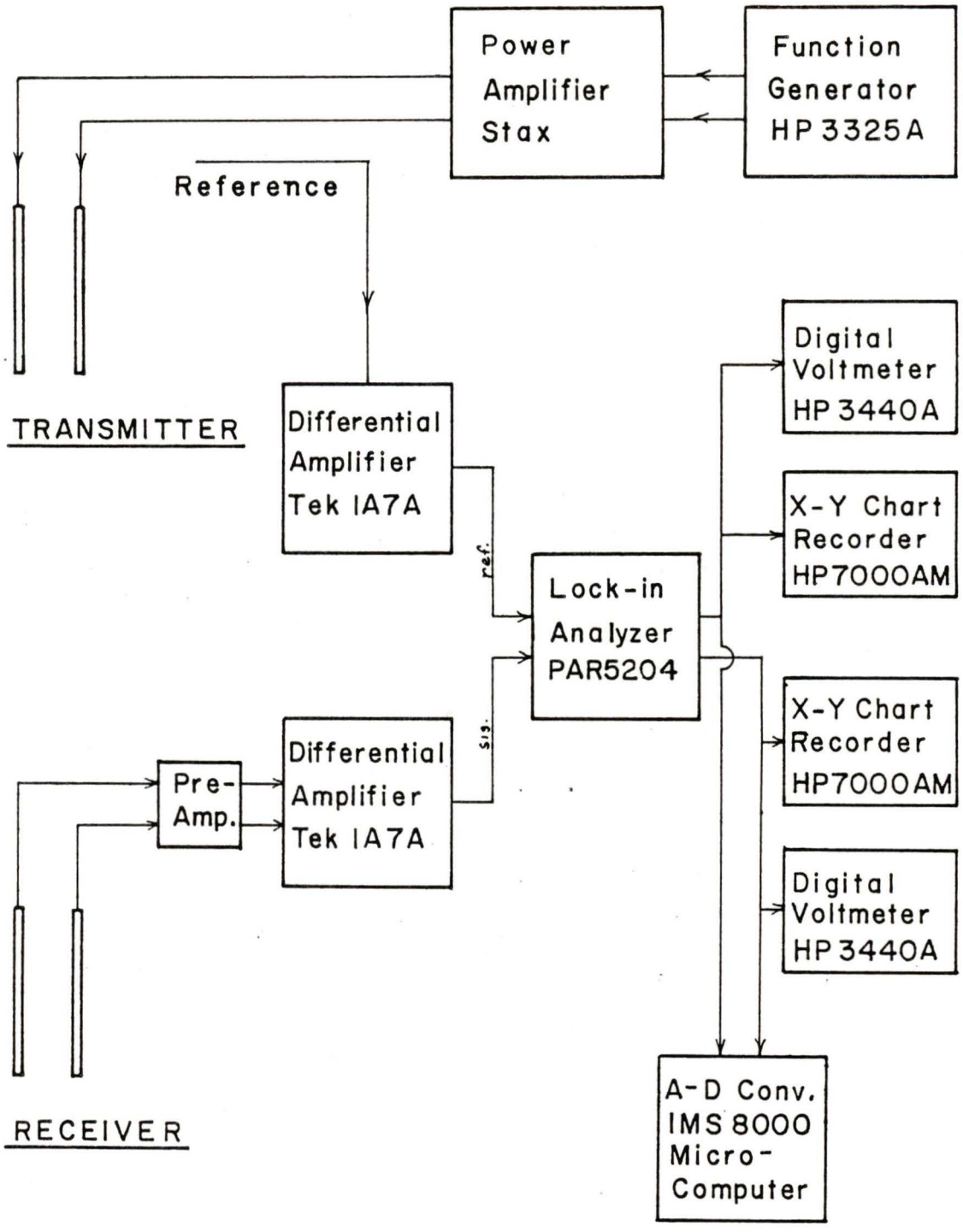

Fig. 5 Transmitter and Receiver Systems for the Laboratory Analogue Modeling Facility

An alternating sinusoidal current of less than one ampere was injected into the brine through the transmitter dipole. This current was provided by a function generator and was amplified by a power amplifier. Small transmitter current densities were necessary to preserve stability and linearity in the measured potentials.

The EM response of the tank system to the transmitter current was registered at the receiver dipole as a phase delayed sinusoidal potential. This signal was amplified by a linear pre-amplifier mounted on the carriage, further amplified by a differential amplifier, and directed to a lock-in analyser. The analyser measured the phase of the signal relative to the transmitter current. The analyser then computed the in phase and out of phase (quadrature) components of the signal. Each component was amplified and directed to an analogue chart recorder and an analogue to digital converter, which sampled the signals for storage on a digital IMS 8000 computer. A detailed description of this laboratory modelling facility is provided by Dosso (1973).

2.3 The Analogue Dike Model

The scale factors used to design the scale laboratory analogue model of a conducting dike in a poorly conducting uniform

host earth are listed in Fig. 6. The dimensions of the dike model are presented in Fig. 7. The conductivity (σ) scale factor is 10^5. Resistivities ($\rho = \frac{1}{\sigma}$) of the graphite dike and brine, at $8 \times 10^{-6} \Omega$-m and $.045 \Omega$-m respectively, simulate an ore body of $.8 \Omega$-m embedded in a uniform host rock of 4500Ω-m. This resistivity contrast is typical of a sulfide ore body in a meta-sedimentary host rock.

With the length scale factor chosen 10^{-4}, one centimenter in the laboratory model simulates 100 m in the geophysical case. The graphite plate simulates a vertical dike 100 m wide by 5.1 km deep and 10 km long. The dike is embedded in the host rock to simulated depths of 300, 500 and 1000 m. The simulated dipole length is 500 m, and the dipole separation is varied for n = 1 to 4.

With the conductivity and linear scale factors selected, the frequency scale factor becomes 10^3. Thus, 1 KHz in the laboratory model simulates 1 Hz in the geophysical case. Spectral IP measurements were made at several discrete frequencies in the simulated range of .25 Hz to 512 Hz.

A more realistic geophysical mineralized dike case would be a 10 m wide dike embedded at depths of 30, 50 and 100 m. In the laboratory simulation, the corresponding length scale factor would be 10^{-3}, determined by the tank dimensions. Unfor-

SCALING CONDITIONS

$$\left(\frac{\sigma}{\sigma'}\right)\left(\frac{F}{F'}\right)\left(\frac{L}{L'}\right)^2 = 1$$

σ = Conductivity

F = Frequency

L = Length

SCALE FACTORS

$$\left(\frac{\sigma}{\sigma'}\right) = 10^5 \quad , \quad \left(\frac{F}{F'}\right) = 10^3 \quad , \quad \left(\frac{L}{L'}\right) = 10^{-4}$$

	Scale Model	Geophysical
Host Res. (Ωm)	4.5×10^{-2}	4.5×10^{3}
Dike Res. (Ωm)	8.0×10^{-6}	8.0×10^{-1}
Frequency (Hz)	$250. - 5.12 \times 10^{5}$	$.25 - 512.$
Length (m)	10^{-2}	10^{2}

FIG. 6 The Scaling Condition and the Scale Factors with their Corresponding Dimensions for the Laboratory Dike Model

DIKE MODEL

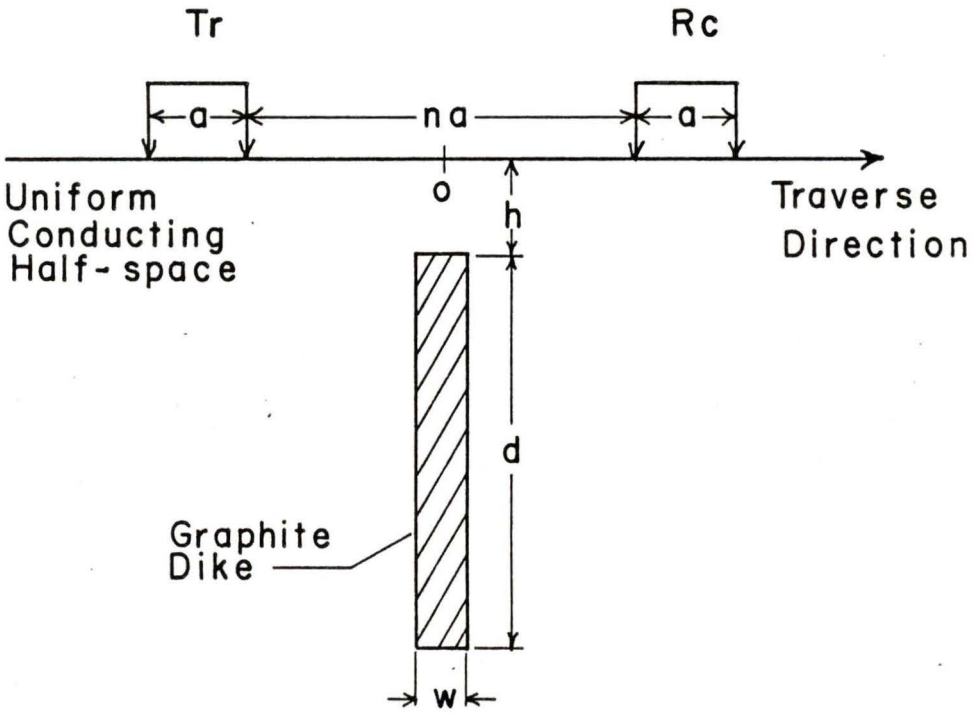

h = 3,5,10 cm

a = 5. cm

d = 51. cm

n = 1,2,3,4

w = 1. cm

f = .25 512 kHz

Traverses Perpendicular to Strike of Dike

Fig. 7 Configuration of the Laboratory Dike Model

tunately, this was not possible due to limitations in the laboratory equipment and materials. The conductivities of the brine and graphite are, for practical purposes, fixed quantities, thus fixing the conductivity scale factor at 10^5. Therefore, in order to satisfy equation (2.23), the frequency scale factor would be determined to be 10. The geophysical frequency range would be simulated by laboratory frequencies of 2.5 Hz to 5.12 KHz, but unfortunately, the minimum frequency attainable in the laboratory, without introducing significant changes in the recording equipment, is 100 Hz. Consequently, it was necessary to use scale factors that would result in the simulation of a larger ore body.

It is important to note that any conclusions concerning the nature of EM coupling over a 100 m wide dike can, in principle, be applied to a 10 m wide dike by the application of a linear scale transformation. There is no loss of generality in using the scale factors for the larger dike.

Since the graphite and brine are good conductors, conduction currents will dominate displacement currents in the laboratory model. Therefore, the permittivities in the laboratory model will be close to the permittivity of free space. Also, the magnetic susceptibilities of graphite and brine are extremely small. Their relative magnetic permeabilities will

be close to unity, and thus, their magnetic permeabilities will be close to that of free space. Consequently, the scale laboratory model of the dike system complies with all three of the scaling conditions developed earlier.

The host earth in the laboratory model is a conducting fluid. The conducting graphite dike has high porosity and high fluid permeability. In addition, the graphite has a negligible metal content. It follows from the discussion in Chapter 1 that there will be negligible electrode and membrane polarization in the model. Consequently, there will be a negligible IP effect and the spectral IP measurements will be composed primarily of EM coupling.

2.4 Summary

To summarize, a geophysical system can be simulated by a laboratory scale model provided that the magnetic permeabilities and permittivities of the two systems are close to the values of free space, and provided that the scale factors satisfy the relation

$$\left(\frac{\sigma}{\sigma'}\right)\left(\frac{\omega}{\omega'}\right)\left(\frac{L}{L'}\right)^2 = 1 \quad . \qquad (2.23)$$

The scale factors used in the analogue scale model of the con-

ducting dike in a uniform conducting earth are

$$\left(\frac{\sigma}{\sigma'}\right) = 10^{5} \quad , \quad \left(\frac{\omega}{\omega'}\right) = 10^{3} \quad , \quad \left(\frac{L}{L'}\right) = 10^{-4} .$$

The dike was simulated by a graphite plate, while the poorly conducting host earth was simulated by brine in a plywood tank. In the geophysical scale, the dike was 100 m wide by 5 km deep and 10 km long, the dipole length was 500 m and the dipole separation was varied for n = 1 to 4. Spectral IP measurements were made in the model for simulated dike depths of 300, 500 and 1000 m, and for discrete simulated frequencies in the range of .25 Hz to 512 Hz. Since the IP effect is negligible for the materials used in the laboratory analogue model, the spectral IP measurements resulted primarily from EM coupling between the probing array and the conducting graphite and brine.

CHAPTER 3

LABORATORY ANALOGUE MODEL MEASUREMENTS

3.1 Analogue Model Measurements

Two sets of spectral IP measurements were obtained using the laboratory analogue model. The first set was obtained over the surface of the brine in the absence of the graphite dike for simulated frequencies of .5, 2, 8, 32 and 128 Hz, and for dipole separations varying from n = 1 to n = 4. The purpose of these measurements was to locate the regions where the spectral IP signal was least affected by the tank walls. The second set of measurements was obtained over the brine with the graphite dike embedded at simulated depths of 300, 500 and 1000 m for 22 simulated frequencies (.25, .5, 1 --- 512 Hz and 10, 20, 30 --- 100 Hz) and for dipole separations varying from n = 1 to n = 4 for each frequency.

Sample measurements over the brine in the absence of the dike at 32 Hz for n = 1 to 4 are illustrated in Fig. 8. The tank walls are denoted by the ends of the traverses. The effects of the tank walls (edge effects) decrease the amplitude of the measured potential. The edge effects increase with increasing dipole separation. As the depth of penetration of

MODEL UNIFORM EARTH MEASUREMENTS

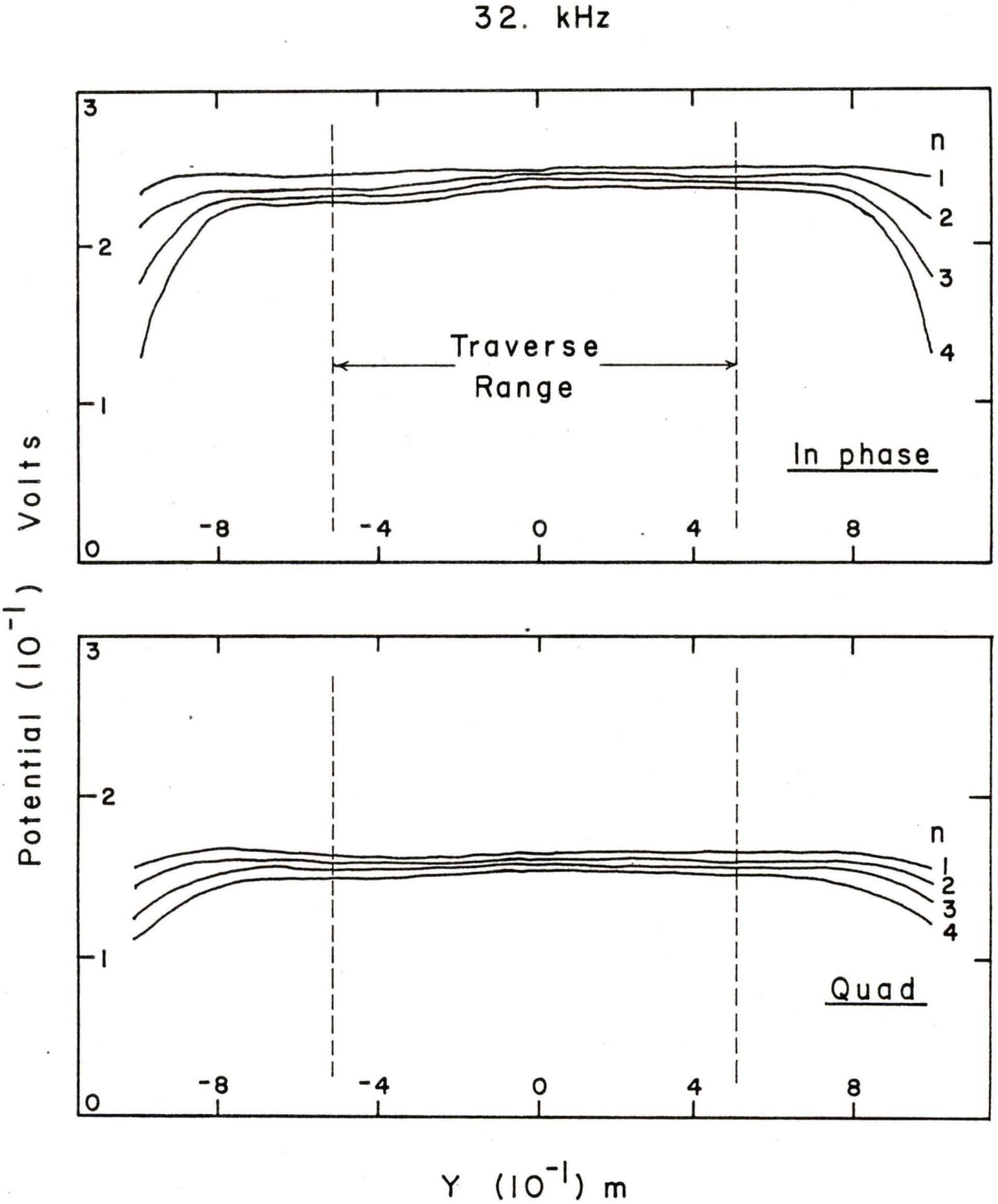

Fig. 8 Measured Potentials for Traverses over the Model Uniform Earth for a Model Frequency of 32 KHz and Dipole Separations of n = 1 to n = 4 (coordinates expressed in model scale)

the probing signal increases, a larger area of the tank walls is exposed to the inducing fields, producing larger edge effects. Measurements over a range of frequencies show that the edge effects decrease with increasing frequency. This can be attributed to the skin depth effect for EM fields propagating in a conducting medium. As the frequency increases, the propagating EM fields become more attenuated, decreasing the depth of penetration into the brine. Consequently, with increasing frequency the distance from the tank wall at which edge effects are observed decreases. All traverses over the brine show a plateau in the region from Y = -50 cm to Y = +50 cm in the model tank, representing the area of minimum edge effects. Measurements over the dike were thus confined to this region.

Model measurements over the dike were normalized at the reference location Y = -50 cm by setting the quadrature component to zero and the in-phase component to .3 volts. The signal in this location was unaffected by the dike, and thus represented the response of the model uniform earth. The purpose of the normalization procedure was to remove the instrument frequency response from the measurements. However, using this normalization procedure at all frequencies and dipole separations also had the unwanted effect of removing any change in the response of the model uniform earth as a function of frequency.

3.2 Analogue Model Measurements for a Poorly Conducting Uniform Earth

The complex impedance of the model earth (V/I, where V is the complex potential at the receiver and I is the transmitter current) was calculated for each frequency and dipole separation at the reference location. These values were compared with calculated values using Sunde's (1949) expressions for the complex impedance of an in-line dipole-dipole array coupled to a uniform earth. The computer programme used to calculate the theoretical values is given in Appendix I. The complex impedances obtained from this programme agree with those tabulated by Millet (1967).

The complex impedance spectrum for the laboratory model earth is compared to the theoretical spectrum, for n = 1, in Fig. 9. The model impedances show a random scatter about the theoretical impedances. The results for n = 2, 3, and 4, though not shown, are similar. The scatter in the model data might be attributed to error in the spacing of the electrodes ($\pm$ .5 cm). The trend in the model values is, however, the same as the trend in the theoretical values, and thus, the brine in the model is taken as an adequate simulation of a uniform poorly conducting host earth.

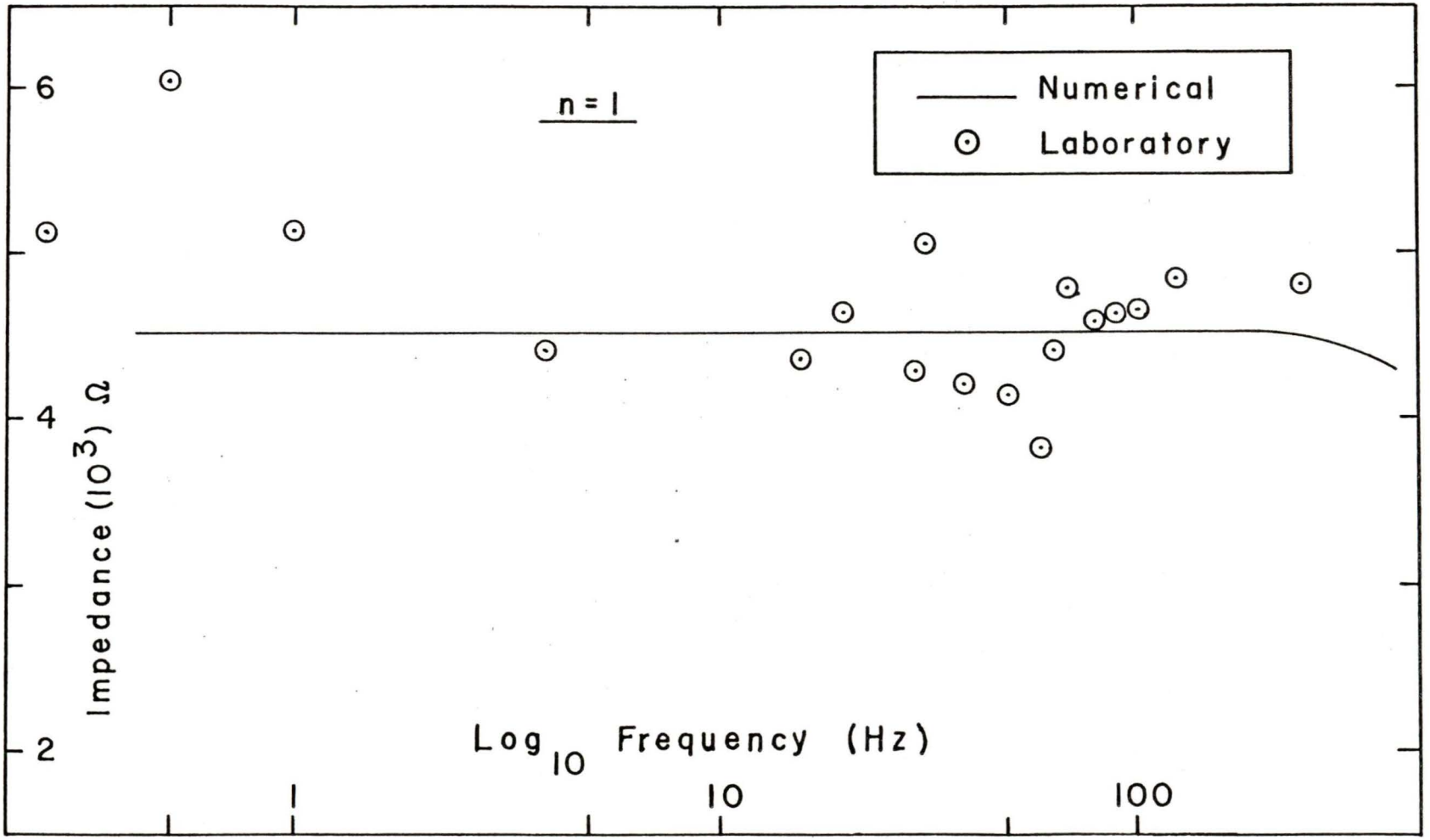

Fig. 9 Complex Impedance Amplitude Spectra for a Uniform Earth for n = 1

3.3 Analogue Model Measurements for a Conducting Dike in a Poorly Conducting Uniform Host Earth

The in-phase and quadrature model measurements for traverses over the dike for simulated frequencies of 10 Hz and 100 Hz, and for dipole separations of n = 1 to n = 4 are shown in Fig. 10. These results show the typical "gull-wing" character of the EM response of a naturally occurring conducting dike (Telford et al. 1981). It is important to recall that the normalization procedure has removed any change in the response of the model uniform earth as a function of frequency. Consequently, any observed anomaly is due entirely to the presence of the conducting dike.

As expected (Fig. 10), the measurements show bi-lateral symmetry over the dike at Y = 0, indicating that the principle of reciprocity is observed in the laboratory analogue model. This follows from the fact that the transmitter and receiver dipoles have the same geometry and that the model itself is bi-laterally symmetrical. Consequently, should the roles of the transmitter and receiver dipoles be reversed, no change in the measured potential would result.

The EM "gull-wing" anomaly over the dike displays several trends. The magnitude of the EM anomaly at a given frequency

SAMPLE TRAVERSES DIKE MODEL

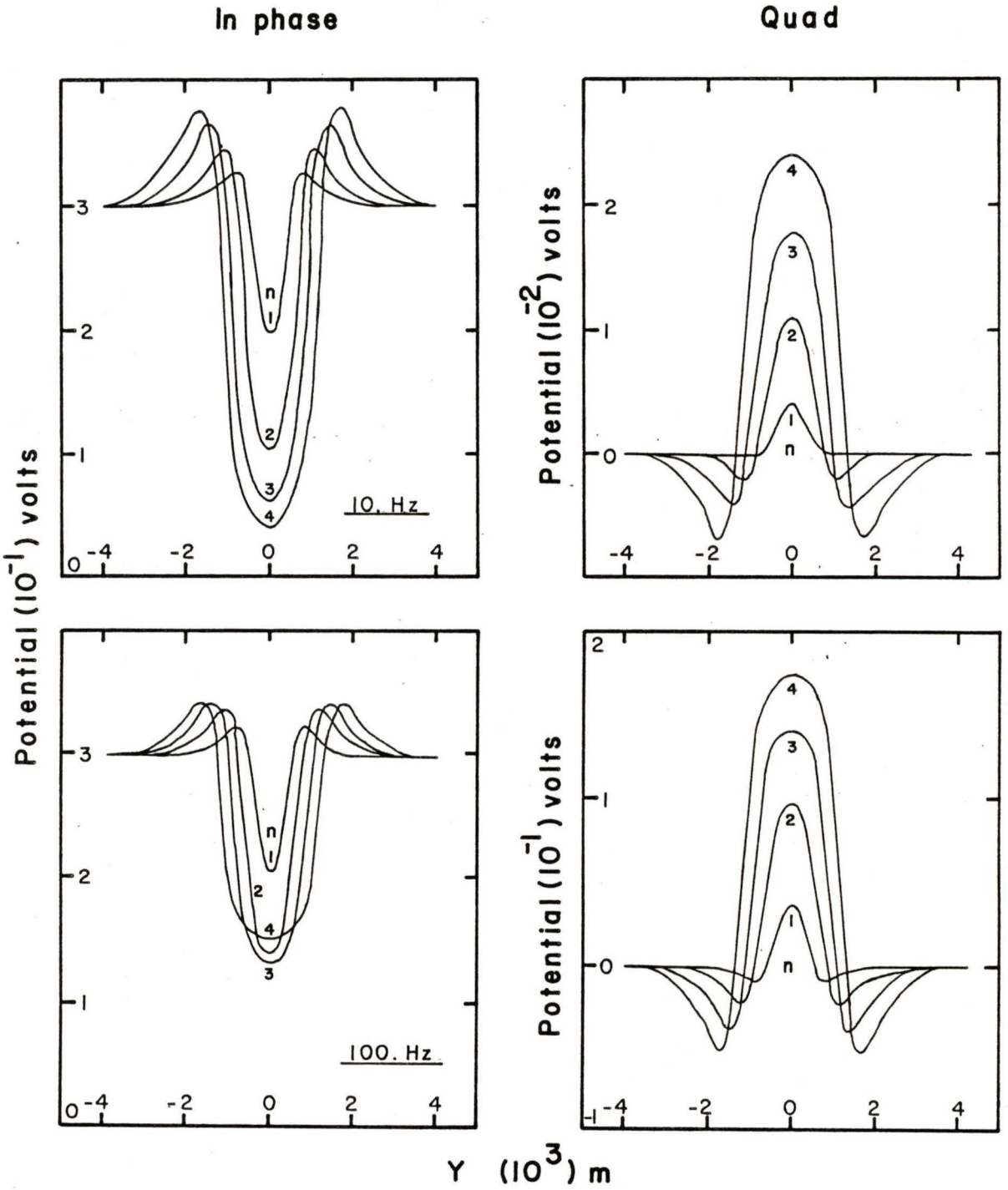

Fig.10 Normalized Spectral IP Measurements for the Laboratory Dike Model for 10 Hz and 100 Hz (geophysical scale) and for n = 1 to n = 4

generally increases with dipole separation; that is, the central trough deepens and the two lateral peaks become higher. This increased anomaly can be attributed to the increased depth of penetration of the probing signal, leading to interaction with deeper parts of the dike in addition to those near the surface.

The distance between the two lateral peaks changes with dipole separation. These peaks occur when either the receiver or the transmitter is over the dike. The eddy currents induced in the dike are maximum when the transmitter is directly over the dike, while the receiver signal is maximum when the receiver is directly over the dike. Reciprocity ensures that these two peaks have the same amplitude.

The magnitude of the "gull-wing" anomaly decreases with increasing frequency. This can be attributed to decreased depth of penetration of the transmitter signal due to the skin depth ($\delta = \sqrt{\frac{2}{\mu\omega\sigma}}$) effect for EM fields propagating in a conducting medium. A decrease in the depth of penetration results in a decrease of the magnitude and depth of eddy currents induced in the dike.

Attenuation due to the skin depth effect also explains the smaller response observed at 100 Hz for n = 4 than for n = 3. Increasing the dipole separation increases the distance

both the inducing and induced EM fields must travel in the attenuating medium. The skin depth of the brine at a model frequency of 10 KHz is 1.1 m, while the skin depth at 100 KHz is 33 cm. If the dipole separation is much less than a skin depth for the brine, the attenuation of the EM fields will not be significant compared to the increase in the magnitude of the EM anomaly associated with the increased depth of penetration. However, as the dipole separation distance approaches the skin depth, the attenuation increases and becomes significant. The minimum dipole separation for this attenuation to be observed decreases with increased frequency. For n = 4, the dipole separation is 20 cm. This represents two-thirds of the skin depth for the brine at 100 KHz, and might result in significant attenuation.

Another characteristic of the EM "gull-wing" anomaly is the increase of the quadrature component with increasing frequency. This illustrates a phase rotation that is a composite of a rotation due to the EM response of the dike, and a rotation that accompanies the skin depth effect.

3.4 Apparent Resistivities for the Analogue Dike Model

As described earlier, the normalization procedure used in collecting the spectral IP measurements removed both the

instrument frequency response and the host earth frequency response. To facilitate numerical modeling of the complete EM coupling effect of a conducting dike embedded in a poorly conducting uniform host earth, it was necessary to re-introduce the contribution of the host earth to the signal.

The normalized potentials can be considered as scaled values of the electric field. The measurement made in the laboratory is that of a potential difference across a pair of electrodes with fixed spacing. This potential difference is proportional to the potential gradient and, therefore, to the electric field intensity;

$$V(y) = a \nabla V(y) = -a E(y) , \qquad (3.1)$$

where 'a' is the dipole length. In the normalization procedure for a given frequency, a multiplicative gain and an additive phase shift are applied to the measured potential in order to attain a .3 volt in-phase signal and a zero quadrature signal at the reference location. The following development (Best, 1983) shows how the normalized potentials along the traverse are related to the un-normalized apparent resistivities.

The scaled values of the electric field along a traverse can be written as (Hohmann, 1971)

$$E_s(y) = E_s^{\circ}(y) + E_s'(y) , \qquad (3.2)$$

where E_s° is the scaled electric field radiated by the host earth and E_s' is the scaled electric field radiated by the dike in the presence of the host earth. The desired unscaled fields can be written as

$$E(y) = E^\circ(y) + E'(y) \quad . \tag{3.3}$$

In polar form, E_s becomes

$$E_s(y) = R_s(y)\, e^{j\theta_s(y)} \quad . \tag{3.4}$$

In the region far from the dike,

$$E_s'(y) \cong 0 \quad , \tag{3.5}$$

and

$$E_{s1} = R_{s1}^\circ\, e^{j\theta_{s1}^\circ} \quad , \tag{3.6}$$

where the subscript 1 refers to the values at the reference location.

In polar form, the unscaled field is

$$E(y) = R(y)\, e^{j\theta(y)} \quad . \tag{3.7}$$

In the region far from the dike,

$$E'(y) \cong 0 \quad ,$$

and

$$E_1(y) = R_1^\circ(y)\, e^{j\theta_1^\circ} \quad , \tag{3.8}$$

the unscaled field radiated by the host earth. Hence, at the reference location, where scaling takes place, E_1 and E_{s1} are related by

$$E_1 = E_{s1}\left(\frac{E_1^\circ}{E_{s1}^\circ}\right) \quad . \tag{3.9}$$

The same scaling condition applies over the length of the traverse. Thus, more generally,

$$E(y) = E_s(y)\left(\frac{E_1^\circ}{E_{s1}^\circ}\right) \quad , \tag{3.10}$$

or

$$R(y)e^{j\theta(y)} = R_s(y)e^{j\theta_s(y)}\left(\frac{R_1^\circ e^{j\theta_1^\circ}}{R_{s1}^\circ e^{j\theta_{s1}^\circ}}\right) \quad , \tag{3.11}$$

yielding

$$R(y) = R_s(y)\left(\frac{R_1^\circ}{R_{s1}^\circ}\right) \quad , \tag{3.12}$$

and

$$\theta(y) = \theta_s(y) + \theta_1^\circ - \theta_{s1}^\circ \quad . \tag{3.13}$$

It should be noted that varying the strength of the transmitter current is equivalent to changing the multiplicative gain of the signal. Since the transmitter current is constant along the traverse, it behaves like a constant scale factor, or constant of proportionality, between the measured potential and the apparent resistivity (equation (1.1)). Thus, from equations (1.1) and (3.1), it can be shown that the electric field intensity is proportional to the apparent resistivity;

$$\rho_a(y) = B \cdot R(y) \quad , \tag{3.14}$$

where B is a real constant. Use (3.12) and (3.14) to obtain

$$\rho_a(y) = R_s(y)\left(\frac{\rho_{a_1}^{\circ}}{R_{s1}^{\circ}}\right) \quad . \tag{3.15}$$

In the laboratory scale model, the proportionality between E and V yields

$$\frac{R_s(y)\, e^{j\theta_s(y)}}{R_{s1}^{\circ}\, e^{\theta_{s1}^{\circ}}} = \frac{V(y)\, e^{j\phi(y)}}{.3\, e^{0.}} \quad , \tag{3.16}$$

where $V(y)\, e^{j\phi(y)}$ is the measured normalized potential, and, as stated earlier, $.3e^{j0}$ is the potential at the reference position. Hence, (3.15) and (3.13) become

$$\rho_a(y) = V(y)\left(\frac{\rho_{a_1}^{\circ}}{.3}\right) \quad , \tag{3.17}$$

and

$$\theta(y) = \phi(y) + \theta_1^{\circ} \quad . \tag{3.18}$$

It is desired that the unscaled values of the apparent resistivity far from the dike be identical to the theoretical values of the apparent resistivity of an in-line dipole-dipole array coupled to a uniform conducting earth at the frequencies and dipole separations of interest. These are the values for $\rho_{a_0}^{\circ}\, e^{j\theta_1^{\circ}}$. These theoretical apparent resistivities were obtained by applying equation (1.1) to the spectrum of complex impedances obtained earlier using the programme in Appendix I. Using equations (3.17) and (3.18), the normalized potentials

measured over the dike were converted to apparent resistivities.

The apparent resistivity for traverses over the dike for simulated frequencies of 10 Hz and 100 Hz are presented in Fig. 11. The apparent resistivity for these traverses displays fundamentally the same structure as the normalized potentials shown in Fig. 10, except that the wings in the apparent resistivity curves show the expected dispersion with frequency and dipole separation due to the frequency dependent EM response of the model uniform conducting host earth. These analogue model apparent resistivities were used in a later section in the present work in developing an analytical expression for EM coupling for a conducting dike embedded in a poorly conducting uniform host earth.

3.5 Summary

Model spectral IP measurements were obtained for a uniform host earth for simulated frequencies of .5, 2, 8, 32 and 128 Hz and for dipole separations of n = 1 to n = 4. These measurements were used to locate the region of the tank least affected by edge effects. Model spectral IP measurements were obtained for a conducting dike embedded at simulated depths of 300, 500 and 1000 m in a uniform poorly conducting host earth for 22

SAMPLE TRAVERSES DIKE MODEL

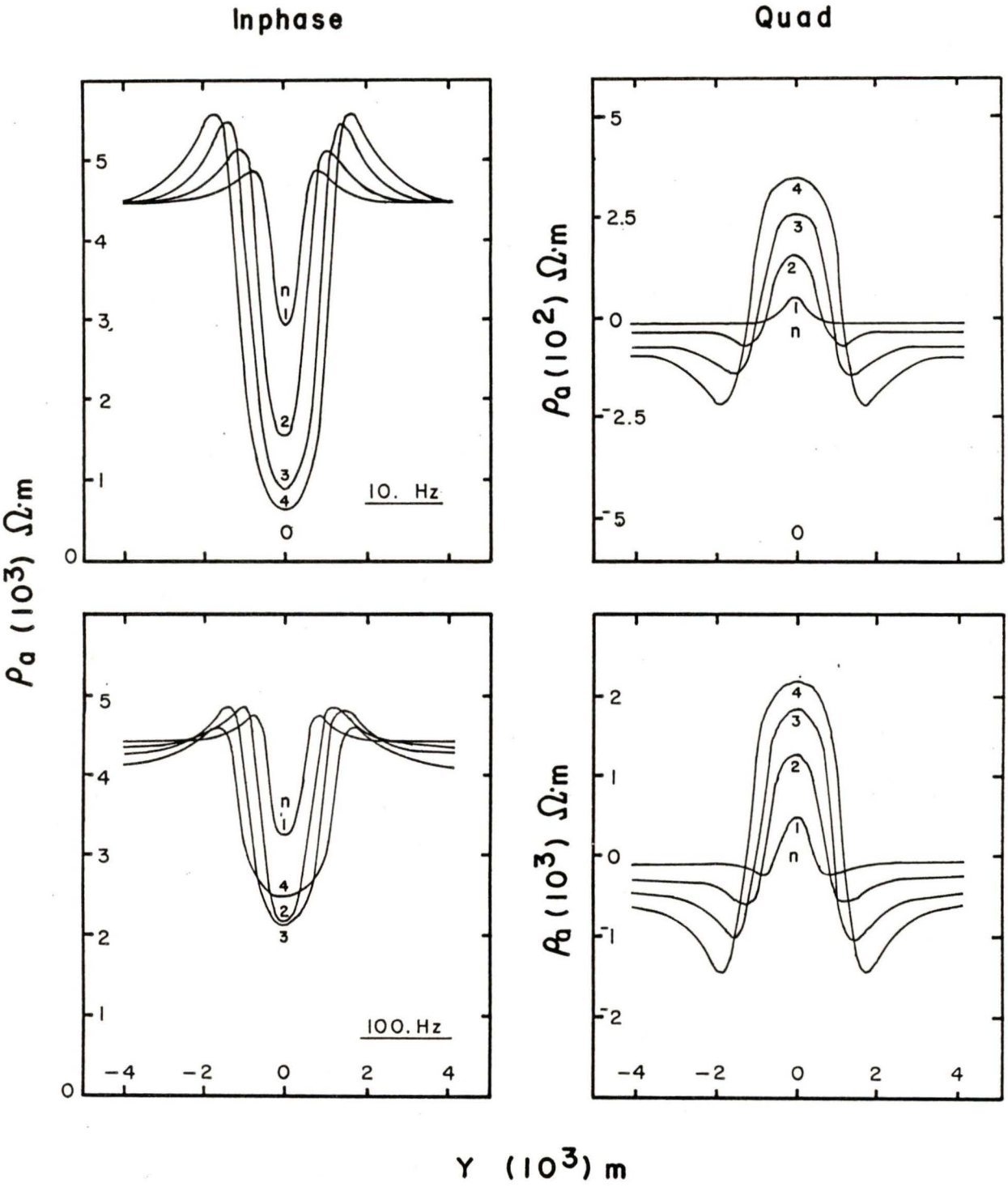

Fig. 11 Apparent Resistivities for the Laboratory Dike Model for 10 Hz and 100 Hz (geophysical scale) and for n = 1 to n = 4

simulated frequencies (.25, .5, 1 --- 512 Hz and 10, 20, 30 --- 100 Hz) and for dipole separations of n = 1 to n = 4. Results for measurements over the dike show the typical "gull-wing" character of the EM response of a naturally occurring conducting dike. The magnitude of the anomaly generally increases with increasing dipole separation and decreases with increasing frequency. Finally, by treating a change in transmitter current as a multiplicative gain, and by treating the normalization procedure as linear scaling, the model normalized potentials were used to obtain apparent resistivities characteristic of both the uniform host earth and the conducting dike.

CHAPTER 4

INVERSION OF LABORATORY MODEL DATA FOR EMPIRICAL MODELS

4.1 Introduction

The use of the Cole-Cole (CC) dispersion in the analysis of spectral IP measurements is currently popular among exploration geophysicists. The CC dispersion is a mathematical expression described by four parameters and one independent variable, frequency, and is written as

$$\rho_a = \rho_{dc}\left(1 - m\left(1 - \frac{1}{1 + (j\omega\tau)^c}\right)\right) \quad . \qquad (4.1)$$

This dispersion, in its original form, was first proposed by Cole and Cole (1941) as an empirical method to describe the complex permittivity spectra displayed by various dielectric materials and was derived from the complex impedance of the equivalent circuit shown in Fig. 12(a). By replacing the capacitors in this equivalent circuit with resistors, an equivalent circuit for the IP effect was obtained (Madden, 1967; Pelton et al, 1978) as shown in Fig. 12(b).

The four parameters of the CC dispersion are the apparent DC resistivity (ρ_{dc}), the apparent chargeability (m), the

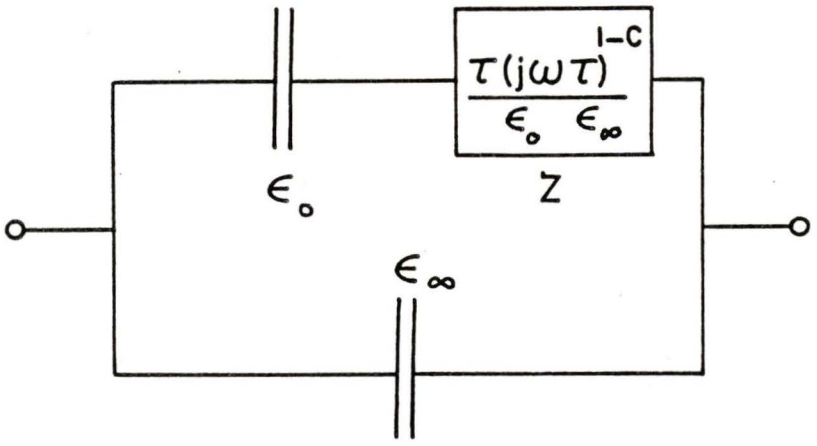

(a) $$\epsilon = \epsilon_\infty + \frac{(\epsilon_o - \epsilon_\infty)}{(1+(j\omega\tau)^{1-c})}, \quad \begin{cases} \tau > 0 \\ 0 < C < 1 \end{cases}.$$

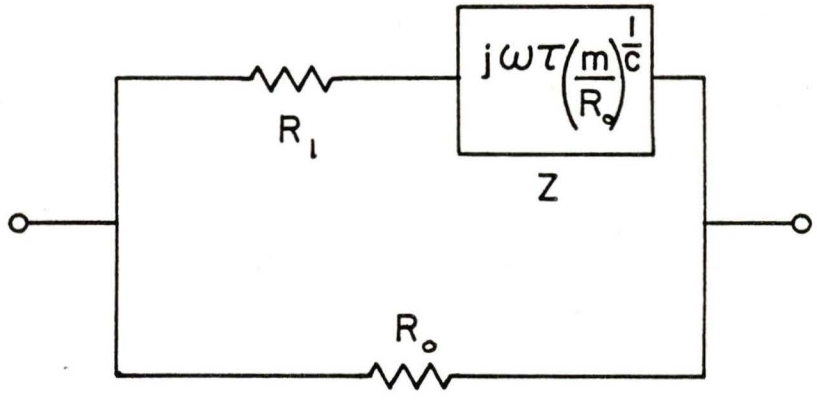

(b) $$\rho_a = \rho_{dc}\left(1 - m\left(1 - \frac{1}{(1+(j\omega\tau)^c)}\right)\right), \quad \begin{cases} \rho_{dc} > 0 \\ 0 < m < 1 \\ \tau > 0 \\ 0 < C < 1 \end{cases}.$$

Fig. 12 Cole-Cole Equivalent Circuits for
(a) Complex Permittivities and
(b) the IP Effect

decay time constant (τ), and the frequency dependence (c). The ranges over which these parameters can vary are also shown in Fig. 12(b). A comprehensive method of interpretation for these parameters is provided by Pelton et al. (1978). In the absence of strong EM coupling, these parameters can be used to discriminate between sulfide based mineral ore bodies and graphite based ore bodies. Pelton et al. (1978) made several successful interpretations of spectral IP measurements collected over widespread disseminated porphyry copper deposits in the south-western United States.

Pelton inverted the apparent resistivity spectra obtained at each station along a traverse using the CC dispersion and a ridge-regression inversion algorithm. The values of the resulting CC parameters were contoured on pseudo-sections. Interpretations of the conductivity structure of the region being surveyed were obtained using the ρ_{dc} pseudo-section, while interpretations of the mineral composition of the region were made using the m and τ pseudo-sections.

Where EM coupling was strong, Pelton et al. (1978) proposed that, for low frequencies, the EM coupling component might be described by a second CC dispersion. Thus, the product of two CC dispersions was used in the inversions: one dispersion to describe the IP effect and the other to describe the EM coupling

effect. It was found that the value of C in the CC dispersion for IP was generally less than .5, while the value of C in the EM coupling dispersion was generally near 1. This was the principal means by which Pelton et al. (1978) discriminated between the two components of the spectral IP signal.

The CC dispersion is an empirical model of EM coupling and is not derivable from fundamental principles of EM induction. One of the objectives in this work was to determine whether the CC dispersion and its derivatives could provide an adequate empirical description of EM coupling in the laboratory analogue dike model. The apparent resistivities for the laboratory analogue model were assembled into spectra for 12 stations along the traverse (Y = -50, -40, -30, -20, -17.5, -15, -12.5, -10, -7.5, -5, -2.5 and 0 cm). Four spectra were assembled at each station, one for each dipole separation. Only one-half of the stations along the traverse were used, due to symmetry in the measurements across the dike. These apparent resistivity spectra were inverted using the Marquardt (1963) algorithm and various empirical models based on the CC dispersion.

4.2 Inversion of the Laboratory Model Apparent Resistivities for a Conducting Dike in a Uniform Conducting Host Earth

A brief calculation shows that the phase of the CC apparent

resistivity is always small and negative, whereas the observed apparent resistivities from the region directly over the dike (Fig. 11) have positive phases (both the in-phase and quadrature components being positive). Hence, a simple CC dispersion is incapable of describing EM coupling in the region close to the dike.

A slight modification of the CC dispersion, made by introducing a fifth parameter 'α' $(0 \leq \alpha \leq 1)$ results in an expression which gives an apparent resistivity with positive phase under certain conditions. This expression is referred to as a generalized Cole-Cole (GCC) dispersion and is written as

$$\rho_a = \rho_{dc}\left(1 - m\left(1 - \frac{1}{(1 + (j\omega\tau)^c)^\alpha}\right)\right) . \qquad (4.2)$$

The results for inverting the spectra for n = 1 at a simulated dike depth of 300 m are presented in Fig. 13(a). A plot of the sum of squared errors Φ as a function of station position is illustrated. As discussed earlier, small values of Φ indicate that parameters were found that give a good fit between the observed and calculated data, while large values of Φ indicate a poor fit.

The GCC provides a good fit to the observed apparent resistivities on the wing of the traverse far from the influence

INVERSION of LABORATORY MODEL DATA

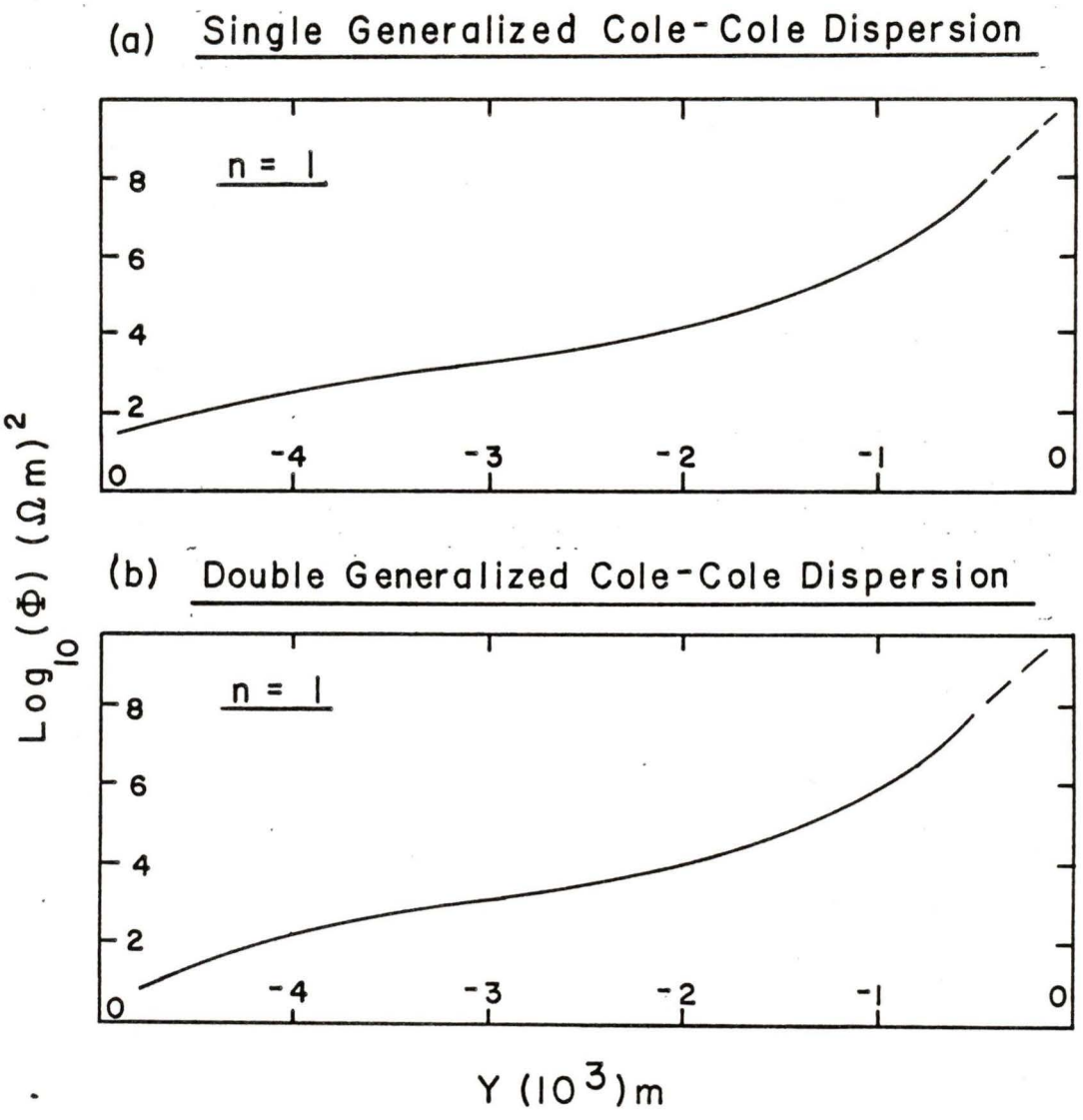

Φ = Sum of Squares Error

$$\Phi = \sum_{i=1}^{N} W_i (F_i \text{ obs.} - F_i \text{ cal})^2$$

Inversion by the Marquardt Algorithm.

Fig.13 Sum of Squared Error Values for Inversions of Laboratory Apparent Resistivity Spectra Along the Traverse Using the Empirical Models:
(a) Generalized Cole-Cole Dispersion
(b) Double Generalized Cole-Cole Dispersion

of the dike. The fit becomes progressively worse as the station location approaches the position of the dike. Φ grows from a value of 10 at the reference location to a value of over 10^8 in the region close to the dike. The order of magnitude of the apparent resistivities in the analogue model is $4 \times 10^3 \Omega m$. Eventually, the difference between these apparent resistivities and the GCC values was so great that the matrices in the inversion programme became ill-conditioned, preventing further calculations in the inversion process along the traverse. This break-down in the calculations occurred in the region where the apparent resistivities of the analogue model were positive. Similar results were obtained for the n = 2, 3 and 4 traverses (not shown). The GCC parameters obtained from these inversions are tabulated in Fig. 14. As in the case of the CC dispersion, the GCC dispersion is incapable of describing EM coupling in the region of the dike.

It has recently been suggested (Klein, 1983) that if a single GCC dispersion failed to describe EM coupling, the product of two GCC dispersions might give enough freedom in the parameters to achieve success. This is referred to here as the double GCC (DGCC) dispersion. The DGCC dispersion is another empirical estimate of EM coupling and is written as

$$\rho_a = \rho_{dc}\left(1 - m_1\left(1 - \frac{1}{(1+(j\omega\tau_1)^{c_1})^{\alpha_1}}\right)\right)\left(1 - m_2\left(1 - \frac{1}{(1+(j\omega\tau_2)^{c_2})^{\alpha_2}}\right)\right). \quad (4.3)$$

The graph of Φ versus station location for the DGCC model in Fig. 13(b) shows that even the DGCC model does not describe EM coupling in the region of positive phase over the dike. It appears, therefore, that the CC dispersion and its derivatives are not appropriate models for describing EM coupling for a conducting body embedded in a uniform host earth.

4.3 Inversion of the Laboratory Model Apparent Resistivities for a Uniform Host Earth

The excellent fits obtained on the wings of the traverses using the GCC and DGCC dispersions indicate that these dispersions can provide a good description of EM coupling for a uniform conducting earth. In Fig. 14(a) the apparent resistivity spectrum of the analogue model for n = 1 at the reference location is compared with the calculated spectra using the GCC and DGCC spectra. The laboratory and calculated spectra are almost indistinguishable. The best fit GCC and DGCC parameters resulting from these inversions are tabulated in Fig. 14(b). Although the analogue model measurements are only accurate to three significant figures, five significant figures are displayed for ρ_{dc} to illustrate the variation in this parameter from one dispersion to the other.

UNIFORM EARTH RESULTS

(a)

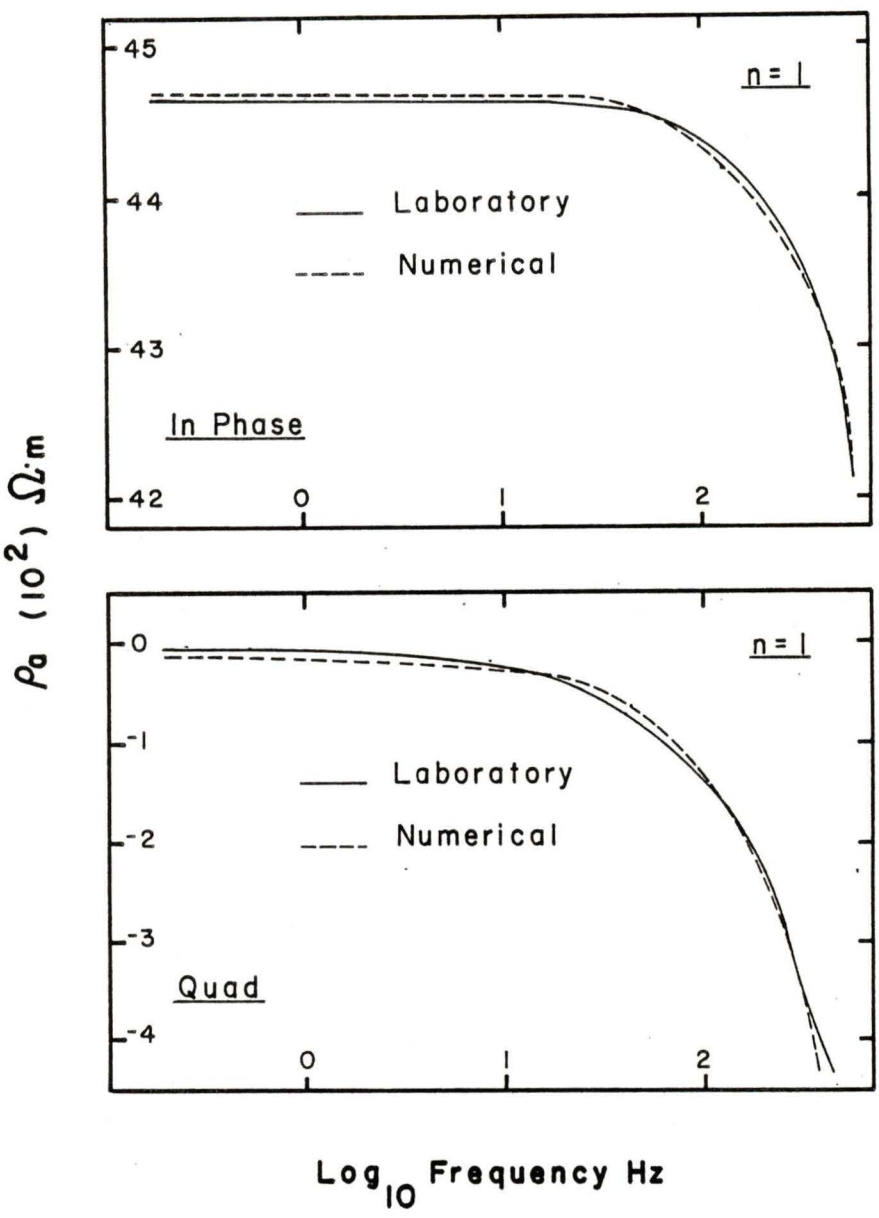

(b) Parameters

	ρ_{dc}	m	τ	c	α	ϕ	se
G-C-C	4468.6	.898	.125E-3	.909	.322	61.2	1.26
D-G-C-C	4466.8	.490	.735E-3	.922	.045		
		.688	.932E-3	.973	.440	1.10	.177

Fig.14 Inversion Results for the Model Uniform Earth showing (a) the Laboratory and Numerical Apparent Resistivity Spectra, and (b) the GCC Dispersion and DGCC Dispersion Parameters Used to Produce the Numerical Apparent Resistivities

This conclusion that the GCC dispersion provides an adequate representation of EM coupling over a uniform earth could explain the successful results obtained by Pelton et al. (1978). The dimensions of the prophyry copper deposits were much greater than the length of the probing array. Consequently, in the vicinity of the survey, the geology was uniform on a macroscopic level, providing a uniform earth in an electromagnetic sense.

4.4 Summary

Various empirical expressions were tested to determine whether they could provide an adequate description of EM coupling in the laboratory analogue dike model. The Cole-Cole dispersion was found to be inappropriate because it yields only apparent resistivities with negative phases. The apparent resistivities of the analogue model display positive phases in the region of the dike. Inversions of model spectra at twelve stations along the traverse (Y = -50, -40 --- -20, -17.5, -15 --- 0 cm) and for dipole separations of n = 1 to 4 were made using a generalized Cole-Cole dispersion and a double generalized Cole-Cole dispersion. Inversion calculations for both dispersions broke down in the region of positive phase over the dike. Good fits were obtained using both

dispersions in regions far from the dike. It was concluded that the Cole-Cole dispersion and its derivatives are not suitable expressions for describing the EM coupling due to a conducting body of finite proportions embedded in a uniform earth. These expressions are better suited to describing EM coupling over a uniform earth.

CHAPTER 5

THE DIPOLE-DIPOLE-LOOP ANALYTICAL MODEL OF THE CONDUCTING DIKE

5.1 Introduction

In this chapter, an analytical expression for EM coupling for a conducting dike embedded in a poorly conducting host earth is developed using the principles of EM induction. It is desirable that at least two advantages be gained using an analytical model of EM coupling rather than an empirical model. Firstly, the analytical model should be designed such that its parameters can be better related to the physical parameters of the dike. Secondly, the analytical model should be designed so that the variation of EM coupling between the array and the dike can be estimated as a function of distance between them. This would allow inversions to be made of apparent resistivities along traverses, as well as of spectra of apparent resitivities, as dealt with in Chapter 3. The analytical model to be developed here is referred to as the Dipole-Dipole-Loop (DDL) model.

In the DDL model, the conducting dike embedded in a poorly conducting host earth is replaced by a conducting loop em-

bedded in a poorly conducting uniform half-space. The configuration of this model is shown in Fig. 15. The time variation of the transmitter EM fields propagating through the half-space induces an electromotive force (EMF) around the loop, which causes an electric current to flow in the loop. This loop current radiates secondary EM fields that are registered at the receiver dipole as a phase delayed potential. The total potential at the receiver is the sum of the primary potential due to EM fields propagated directly from the transmitter through the half-space and the secondary potential due to EM fields that are radiated by the current induced in the loop and also propagate through the half-space. The primary potential is given by the EM coupling response of the uniform earth, discussed earlier.

5.2 Mathematical Development of the Dipole-Dipole-Loop Model

In the DDL model (Fig. 15), the transmitter and receiver dipoles have length 'a', and are separated by a distance 'na', where 'n' is an integer. The loop has a width 'w', a depth extent 'd', and is embedded in the conducting half-space to a depth 'h'. The origin of coordinates is located at the surface over the centre of the loop. The position of the array with respect to the loop is given by x_o, which is positive when the mid-point of the array is to the right of the origin.

DIPOLE – DIPOLE – LOOP MODEL

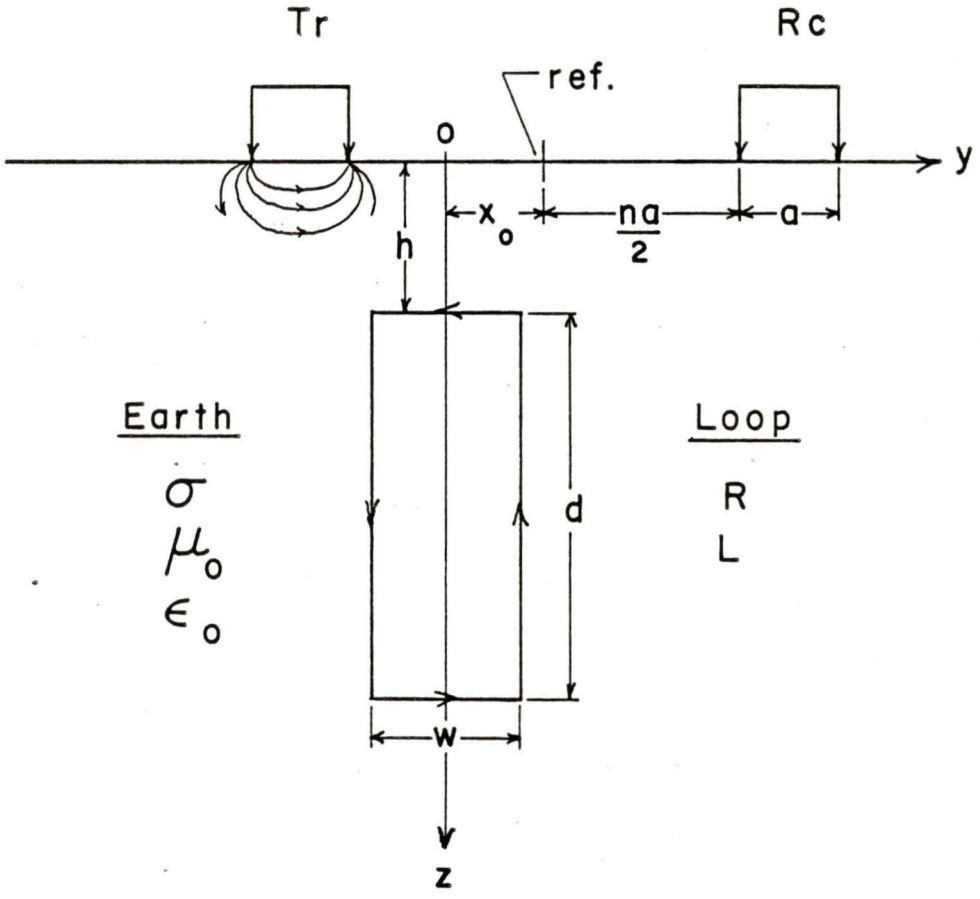

Quasi-static range , $k^2 = j\omega\mu\sigma$

Parameters h , d , w , R , L

Fig.15 Configuration of the Dipole-Dipole-Loop Model

The half-space containing the loop has a conductivity σ and the permeability of free space μ_o. It is assumed that displacement currents are negligible. Hence, if the time dependencies of the currents and EM fields are of the form $e^{j\omega t}$, then the quasi-static approximation can be made, and the propagation constant k for the conducting half-space is of the form

$$k^2 = j\omega\mu_o\sigma \quad , \tag{5.1}$$

where ω is the angular frequency of variation.

A sinusoidal alternating current is injected into the conducting half-space at the transmitter and establishes a propagating EM field in the half-space. The time variation of the flux of the magnetic component of this field linking the loop induces an EMF around the loop. This EMF can be expressed in terms of the transmitter electric field as

$$EMF = \oint_{\text{around loop}} \underline{E} \cdot d\underline{l} \quad , \tag{5.2}$$

where the line integral is performed counter clockwise around the loop. In the DDL model coordinates, (5.2) becomes

$$\mathcal{E}MF = \int_{z=h}^{h+d} E_z \Big|_{x=-\frac{W}{2}} dz + \int_{x=-\frac{W}{2}}^{\frac{W}{2}} E_x \Big|_{z=h+d} dx$$

$$+ \int_{z=h+d}^{h} E_z \Big|_{x=\frac{W}{2}} dz + \int_{x=\frac{W}{2}}^{-\frac{W}{2}} E_x \Big|_{z=h} dx \quad . \qquad (5.3)$$

Wait (1983) showed that the EM fields of an insulated wire, carrying a current I and connected to a conducting medium at its two ends, can be obtained by constructing the wire with a string of point electric dipoles of strength $I\,ds$. The EM fields of the grounded wire are given by the superposition of the EM fields of the point electric dipoles. In this manner, the EM fields of the transmitter are obtained by superposing the EM fields of a string of horizontal point electric dipoles at the surface of the conducting half-space. The electric field of one of these point dipoles is written as

$$\underset{\sim}{E}_{hp} = I\,ds\ \underset{\sim}{\mathcal{E}}_T(x, z) \quad , \qquad (5.4)$$

and is well known (Ward, 1967). The expressions for $\underset{\sim}{\mathcal{E}}_T$ are given in Appendix II(a). Using (5.4), the transmitter electric field becomes

$$\underset{\sim}{E}(x, z) = \int_{s=x_o-\frac{ng}{2}-a}^{x_o-\frac{ng}{2}} I\ \underset{\sim}{\mathcal{E}}_T(x-s, z)\, ds \quad , \qquad (5.5)$$

where S is a position coordinate of a point electric dipole and varies over the length of the transmitter as shown in Fig. 16(a). Using (5.5) in (5.3) yields

$$\begin{aligned}
\mathcal{EMF} = & \int_{z=h}^{h+d} \int_{s=x_0-\frac{ng}{2}-a}^{x_0-\frac{ng}{2}} I\ \mathcal{E}_{Tz}\left(-\tfrac{w}{2}-s, z\right) ds\, dz \\
& + \int_{x=-\frac{w}{2}}^{\frac{w}{2}} \int_{s=x_0-\frac{ng}{2}-a}^{x_0-\frac{ng}{2}} I\ \mathcal{E}_{Tx}\left(x-s, h+d\right) ds\, dx \\
& + \int_{z=h+d}^{h} \int_{s=x_0-\frac{ng}{2}-a}^{x_0-\frac{ng}{2}} I\ \mathcal{E}_{Tz}\left(\tfrac{w}{2}-s, z\right) ds\, dz \\
& + \int_{x=\frac{w}{2}}^{-\frac{w}{2}} \int_{s=x_0-\frac{ng}{2}-a}^{x_0-\frac{ng}{2}} I\ \mathcal{E}_{Tx}\left(x-s, h\right) ds\, dx\ ,
\end{aligned} \tag{5.6}$$

or

$$\begin{aligned}
\mathcal{EMF} = & I \int_{z=h}^{h+d} \int_{s=x_0-\frac{ng}{2}-a}^{x_0-\frac{ng}{2}} \left(\mathcal{E}_{Tz}\left(-\tfrac{w}{2}-s, z\right) - \mathcal{E}_{Tz}\left(\tfrac{w}{2}-s, z\right)\right) ds\, dz \\
& + I \int_{x=-\frac{w}{2}}^{\frac{w}{2}} \int_{s=x_0-\frac{ng}{2}-a}^{x_0-\frac{ng}{2}} \left(\mathcal{E}_{Tx}\left(x-s, h+d\right) - \mathcal{E}_{Tx}\left(x-s, h\right)\right) ds\, dx\ .
\end{aligned} \tag{5.7}$$

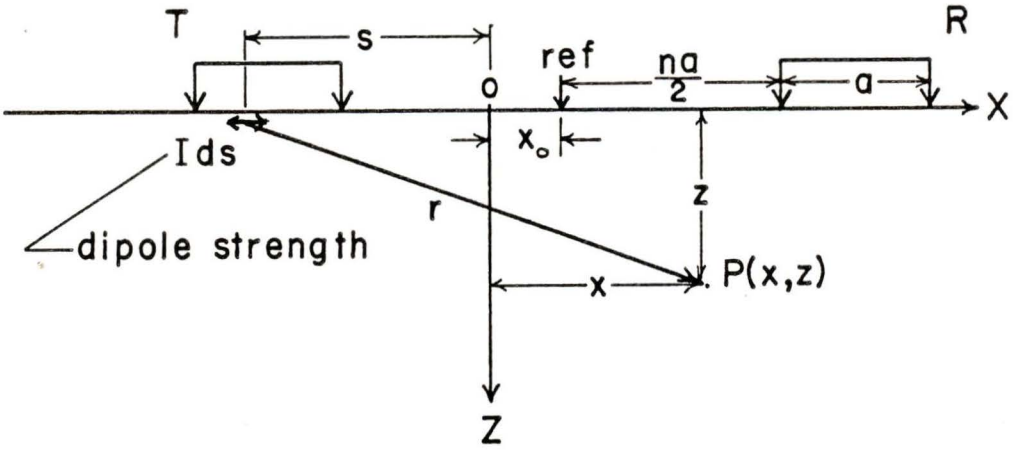

Fig.16 (a) Sub-surface Electric Field of a String of Horizontal Point Electric Dipoles of Surface

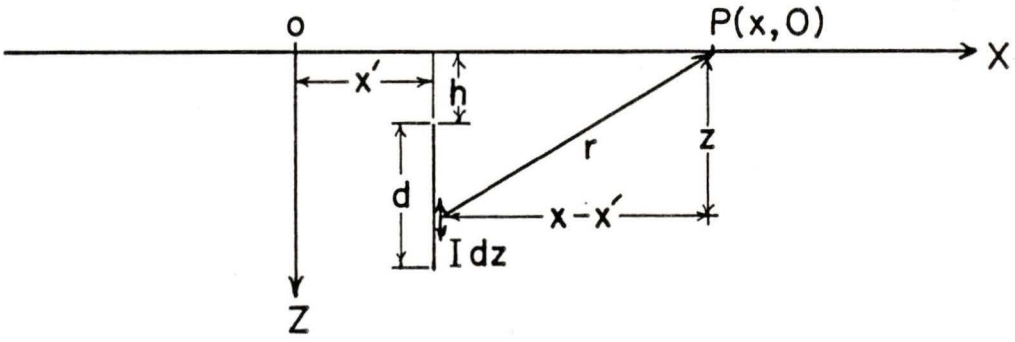

(b) Surface Electric Field of a String of Vertical Point Electric Dipoles Sub-surface

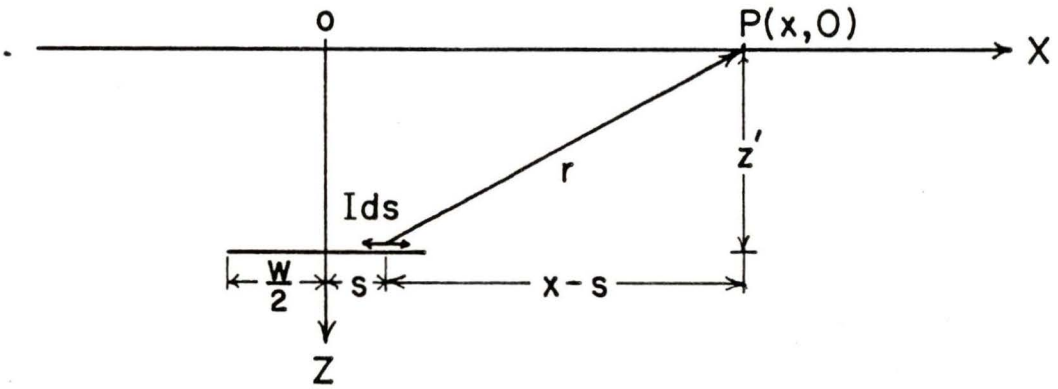

(c) Surface Electric Field of a String of Horizontal Point Electric Dipoles Sub-surface

If the first double integral in (5.7) is labeled J_z and the second J_x, then (5.7) can be written in short form as

$$EMF = I\,(J_x + J_z) \quad . \tag{5.8}$$

To obtain the current (I_L) that flows in the loop in response to the induced EMF, the loop is treated as a simple R - L circuit, with a resistance R and a self-inductance L (Grant & West, 1965). Thus, I_L satisfies the first order differential equation

$$EMF + I_L R + L\frac{dI_L}{dt} = 0. \tag{5.9}$$

Since the expression for the EMF involves the sinusoidal transmitter current, a sinusoidal loop current can be assumed with a time dependence of $e^{j\omega t}$. Hence, the solution to (5.9) is

$$I_L = -\frac{(J_z + J_x)}{(R + j\omega L)} \cdot I \quad . \tag{5.10}$$

It is important to note here that the mutual inductance between the current loop and the conducting half-space is ignored. In the quasi-static frequency range, this effect should be small, since the mutual inductance will involve the factor $j\omega$ which is small for small frequencies. Where the dike is concerned, this assumption means that the presence of the dike does not disturb the primary transmitter fields. This is not necessarily correct; but the assumption is required in order to facilitate the mathematical analysis of the model. This in-

accuracy is not of concern since the purpose of the DDL model is to provide only an estimate of EM coupling that is easily calculated, not necessarily the exact solution.

In general, R and L are functions of the dimensions of the loop and its configuration in the half-space. Whereas the development of the expression for R presents no undue complexity, the expression for L is somewhat more complex and requires knowledge of the mutual inductance that has been ignored. For the purpose of this work, R and L were left as general parameters, whose values would be determined by an inversion process.

The EM fields radiated by the loop current are obtained in a manner similar to that used to obtain the EM fields of the transmitter current. The loop is constructed of four strings of point electric dipoles of strength $I_L ds$. The electric field of a vertical point electric dipole embedded in a conducting half-space is given as

$$\underset{\sim}{E}_v = I_L \, ds \, \underset{\sim}{\xi}_v \quad . \tag{5.11}$$

Similarly, the electric field of an embedded horizontal point electric dipole is

$$\underset{\sim}{E}_H = I_L \, ds \, \underset{\sim}{\xi}_H \quad . \tag{5.12}$$

The expressions for $\underset{\sim}{\xi}_v$ and $\underset{\sim}{\xi}_H$ are given in Appendix II(b) and

II(c) and were obtained from Wait (1961) and Weaver (1967) respectively.

Consider a field point $(P(x,0))$ on the surface of the conducting half-space in the region of the receiver dipole, as shown in Fig. 16(b). The electric field at this point for a string of vertical point electric dipoles located at a depth h and position $x-x'$ is

$$\underset{\sim}{E}_v(x) = \int_{z=h}^{h+d} I_L \, \underset{\sim}{\mathcal{E}}_v(x-x', z) \, dz \quad . \tag{5.13}$$

As shown in Fig. 16(c), the electric field at a similar point for a string of horizontal point electric dipoles embedded at a depth z' below the origin is

$$\underset{\sim}{E}_H(x) = \int_{s=-\frac{w}{2}}^{\frac{w}{2}} I_L \, \underset{\sim}{\mathcal{E}}_H(x-s, z') \, ds \quad . \tag{5.14}$$

Hence, the total electric field at $P(x,0)$ due to the four strings of point electric dipoles that comprise the embedded loop is written as

$$E_2(x,0) = \int_{z=h}^{h+d} I_L \underset{\sim}{\mathcal{E}}_v\left(x-\tfrac{-W}{2}, z\right) dz$$

$$+ \int_{s=-\frac{W}{2}}^{\frac{W}{2}} I_L \underset{\sim}{\mathcal{E}}_H(x-s, h+d)\, ds$$

$$+ \int_{z=h+d}^{h} I_L \underset{\sim}{\mathcal{E}}_v\left(x-\tfrac{W}{s}, z\right) dz$$

$$+ \int_{s=\frac{W}{2}}^{-\frac{W}{2}} I_L \underset{\sim}{\mathcal{E}}_H(x-s, h)\, ds \quad , \tag{5.15}$$

where the integration is performed around the loop in the direction of the induced current (assumed to be counter-clockwise). Equation (5.15) can be re-written as

$$E_2(x,0) = I_L \int_{z=h}^{h+d} \left(\underset{\sim}{\mathcal{E}}_v\left(x+\tfrac{W}{2}, z\right) - \underset{\sim}{\mathcal{E}}_v\left(x-\tfrac{W}{2}, z\right)\right) dz$$

$$+ I_L \int_{s=-\frac{W}{2}}^{\frac{W}{2}} \left(\underset{\sim}{\mathcal{E}}_H(x-s, h+d) - \underset{\sim}{\mathcal{E}}_H(x-s, h)\right) ds \quad . \tag{5.16}$$

The potential induced at the receiver by the electric

field radiated by the loop current is given by

$$V_2 = -\int_{\text{receiver}} \underset{\sim}{E}_2 \cdot d\underset{\sim}{l} \quad , \text{ but } \quad d\underset{\sim}{l} = dx\,\hat{i} \quad . \tag{5.17}$$

Therefore,

$$V_2 = -\int_{x=\,x_0+\frac{ng}{2}}^{x_0+\frac{ng}{2}+a} E_{2x}(x)\,dx \quad , \tag{5.18}$$

or, using equation (5.16),

$$V_2 = -I_L \int_{z=h}^{h+d} \int_{x=\,x_0+\frac{ng}{2}}^{x_0+\frac{ng}{2}+a} \left(\mathcal{E}_{vx}\left(x+\tfrac{w}{2},z\right) - \mathcal{E}_{vx}\left(x-\tfrac{w}{2},z\right)\right) dx\,dz$$

$$- I_L \int_{s=-\frac{w}{2}}^{\frac{w}{2}} \int_{x=x_0+\frac{ng}{2}}^{x_0+\frac{ng}{2}+a} \left(\mathcal{E}_{Hx}(x-s,h+d) - \mathcal{E}_{Hx}(x-s,h)\right) dx\,ds \quad . \tag{5.19}$$

If the first double integral in (5.19) is labeled V_v and the second V_H, then (5.19) can be expressed in short form as

$$V_2 = -I_L \left(V_v + V_H \right) \quad . \tag{5.20}$$

Using equation (5.11) in (5.20) gives

$$V_2 = \frac{(J_x + J_z)(V_v + V_H)}{(R + j\omega L)} \cdot I \quad , \tag{5.21}$$

the secondary potential for EM coupling between the array and the loop subject to the conducting host earth.

As discussed earlier, the primary potential (V_1) registered at the receiver is given by the EM coupling between the array and the uniform conducting earth, thus yielding a total potential

$$V = V_1 + V_2 \quad . \tag{5.22}$$

By applying equation (1.1) to (5.22), the receiver potential is converted to an apparent resistivity; that is,

$$\rho_a = \rho_{a_1} + \rho_{a_2} \quad , \tag{5.23}$$

where ρ_{a_1} is given by the values for EM coupling for a uniform earth computed in Chapter 3 and ρ_{a_2} is given by

$$\rho_{a_2} = \pi n(n+1)(n+2)a \frac{(J_x + J_z)(V_v + V_H)}{(R + j\omega L)} \tag{5.24}$$

Equations (5.23) and (5.24) comprise the DDL model of EM coupling for the dike problem.

There are five parameters in the DDL model: the depth 'h' of the loop, the width 'w', the depth extent 'd', the resistance R and the self-inductance L. The two independent variables in the model are frequency (ω) and the position (x_o)

of the dipole array with respect to the loop. Both apparent resistivity traverses and spectra can, therefore, be calculated with the DDL model. As will be discussed in the next chapter, the DDL model was used in inversions of the laboratory analogue model apparent resistivities to determine whether the DDL model could provide a more accurate description of EM coupling in the dike problem than the empirical models used in Chapter 4.

5.3 Summary

The Dipole-Dipole-Loop (DDL) model is an analytical model of EM coupling for a conducting dike embedded in a uniform conducting host earth. In the DDL model, the dike is replaced by a conducting loop, coplanar with the array dipoles. EM coupling for this model is derived using the principles of EM induction. All linear current elements in the DDL model were treated as strings of point electric dipoles. The expressions for the EM fields of point electric dipoles embedded in or at the surface of a conducting uniform half-space are well known. The apparent resistivity for the DDL model can be written in short form as

$$\rho_a = \rho_{a_1} + \pi n(n+1)(n+2)\, a\, \frac{(J_x + J_z)(V_v + V_H)}{(R + j\omega L)} \,,$$

where J_x, J_z, V_V and V_H are double integrals dependent on the array-loop configuration and ρ_{a1} is the apparent resistivity of the uniform half-space. The DDL model has two independent variables: transmitter frequency (ω) and the position (x_o) of the array with respect to the loop. The DDL model is described by five parameters: the depth of the loop 'h', the width 'w', the depth extent 'd', the resistance R and the self-inductance L. The DDL model was designed so that these parameters could be given values through an inversion process.

CHAPTER 6

INVERSION OF THE LABORATORY MODEL DATA FOR THE ANALYTICAL DIPOLE-DIPOLE-LOOP MODEL

6.1 Introduction

A computer programme was written to calculate the apparent resistivities for the DDL model. These apparent resistivities displayed similar characteristics to those of the laboratory dike model. The DDL apparent resistivities exhibited a "gull-wing" anomaly, along the traverse. The anomaly was symmetrical about the origin directly over the loop. Its magnitude decreased with increasing frequency and increased with increasing dipole separation, as in the case of the anomaly observed in the laboratory model traverses. The character of the DDL "gull-wing" depended heavily on the values chosen for the DDL (dike-loop) parameters. The purpose of this part of the work was to invert the laboratory model apparent resistivities and thus to find those dike-loop parameters that would give the closest agreement between the DDL model apparent resistivities and the laboratory dike model apparent resistivities.

Eight seconds of CPU time was required to compute the value of one DDL apparent resistivity on an IBM VM370 mainframe computer. This is an expensive calculation. The speed of the calculation could be greatly improved by using more sophisticated programming techniques for computing the double integrals in equation (5.24). In anticipation of these improvements, a copy of the DDL programme was not included in this report.

Since the DDL model is a function of frequency, array position and dipole separation, a single inversion could have been made using the entire laboratory dike model data set to obtain a single set of dike-loop parameters. However, due to the high cost of the calculations, such an inversion could not be attempted. Instead, a number of inversions of smaller subsets of the laboratory data were made. Since the DDL apparent resistivities displayed a larger variation with array position than with frequency, inversions were made of values along traverses. The laboratory dike model apparent resistivity was sampled at twelve stations (Y = -50, -40 --- -20, -17.5, -15 --- 0 cm) along the traverse and inverted using the Marquardt (1963) algorithm. Inversions were made along traverses at simulated frequencies of 1, 10, 50 and 100 Hz and for dipole separations of n = 1 to n = 4 and a single simulated dike depth of 300 m.

Several trends in the dike-loop parameters were expected from these inversions. Little variation with frequency was expected in the geometric dike-loop parameters (h, d, w), since these are closely related to the constant dimensions of the dike. The values for 'h' were expected to be close to the simulated dike depth at 300 m, since this was the upper limit of eddy currents induced in the dike. Similarly, 'w' was expected to be close to the simulated dike width of 100 m. Since the effective depth of penetration of the signal was one-half the dipole separation, at n = 4, the eddy currents should have been confined to the top 1000 m of the dike. Consequently, 'd' was expected to be near this value. Some variation with frequency of the electrical dike-loop parameters (R and L) was anticipated because these parameters were used to form the complex impedance of the loop in which mutual inductance between the loop and the half-space was ignored. A variation of R and L with frequency would be necessary to account for the increased significance of the mutual inductance with increasing frequency. R was expected to be more significant than L in determining the strength of the induced loop current in the quasi-static frequency range, and hence in determining the magnitude of the EM coupling response of the loop. Consequently, L was expected to be smaller than R by at least one order of magnitude. As discussed below, most of

these expected trends were in fact observed in the inversion results.

6.2 Inversion Results for the Laboratory Dike Model Data Using the Dipole-Dipole-Loop Model

Laboratory model inversion results for the DDL model are shown in Fig. 17 and Fig. 18 for simulated frequencies of 10 Hz and 100 Hz, and for dipole separations of n = 1 and n = 4. The best fit dike-loop parameters used to obtain the DDL apparent resistivities shown in these figures are:

$h = 300$ m, $d = 349$ m, $w = 200$ m, $R = .11 \times 10^{-5}\Omega$,
$L = .79 \times 10^{-9}$ Henries for n = 1 at 10 Hz,
$h = 697$ m, $d = 616$ m, $w = 146$ m, $R = .22 \times 10^{-6}\Omega$,
$L = .15 \times 10^{-9}$ Henries for n = 4 at 10 Hz,
$h = 310$ m, $d = 119$ m, $w = 283$ m, $R = .27 \times 10^{-4}\Omega$,
$L = .15 \times 10^{-7}$ Henries for n = 1 at 100 Hz and
$h = 856$ m, $d = 576$ m, $w = 102$ m, $R = .94 \times 10^{-5}\Omega$,
$L = .97 \times 10^{-8}$ Henries for n = 4 at 100 Hz.

Only one-half of the traverse is illustrated, since the results are symmetrical about the origin. These results show excellent agreement between the DDL and laboratory model apparent resistivities. The standard error of fit (SE), given by the square root of the sum of squared errors Φ, is 153 Ω-m for

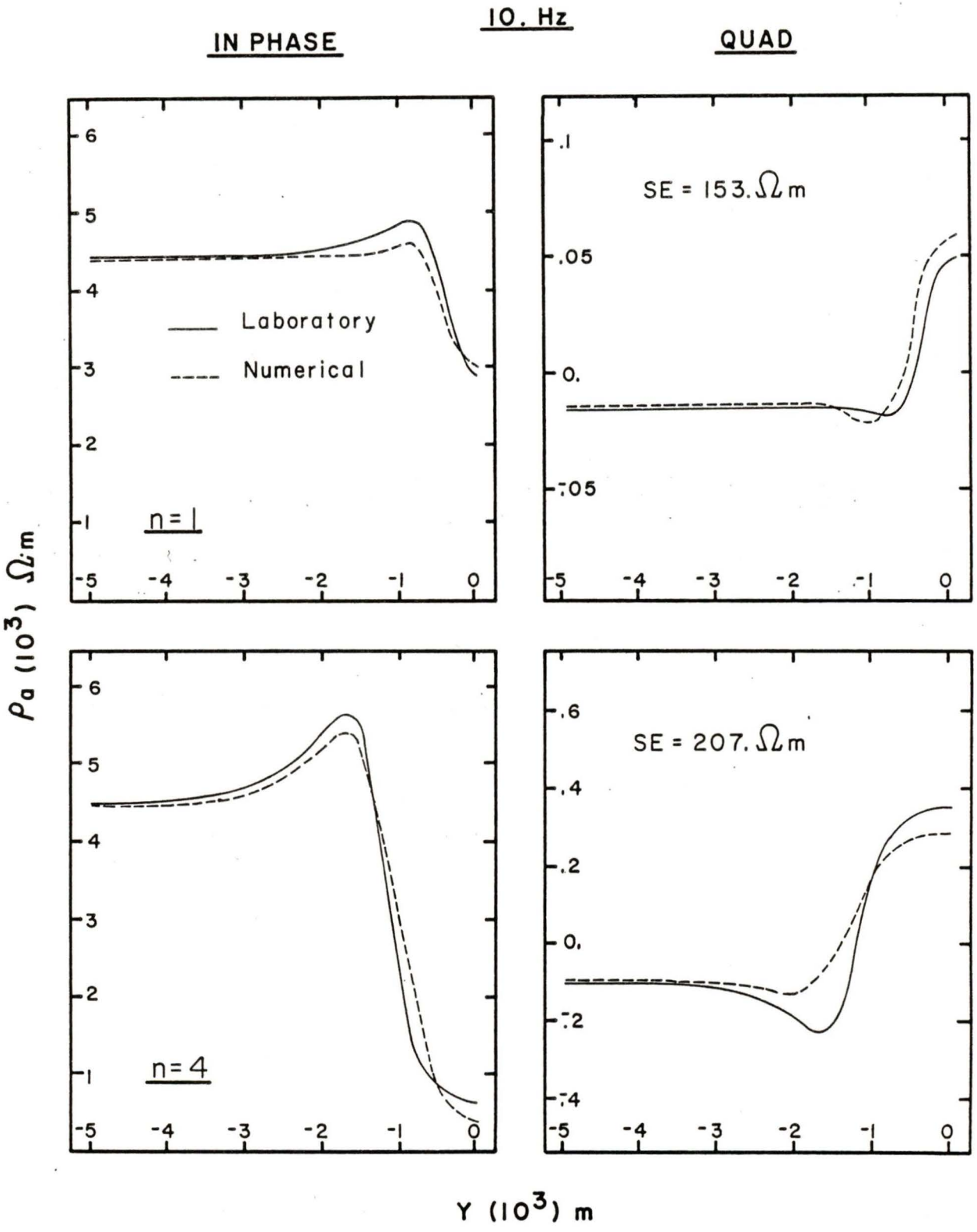

FIG. 17 Laboratory ρ_a and DDL Model ρ_a at 10 Hz for n=1 (dike-loop parameters: h=300 m, d=349 m, w=200 m, R=.11 x $10^{-5}\Omega$ L=.79 x 10^{-4} Henries), for n=4 (dike-loop parameters: h=697 m, d=616 m, w=146 m, R=.22 x $10^{-6}\Omega$, L=.15 x 10^{-9} Henries), and for a dike depth of 300 m.

"DIKE-LOOP" RESULTS

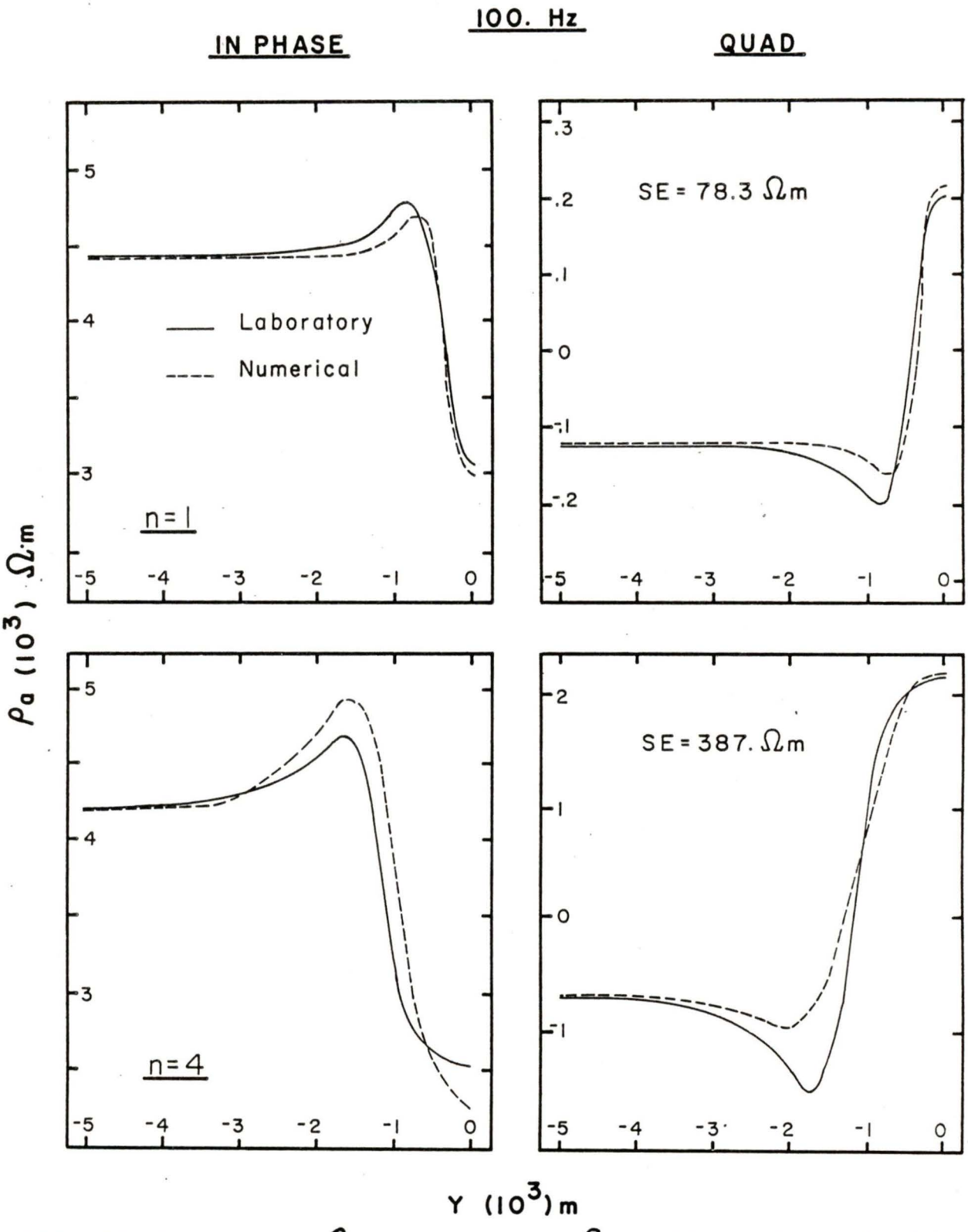

FIG. 18 Laboratory ρ_a and DDL Model ρ_a at 100 Hz for n=1 (dike-loop parameters: h=310 m, d=119 m, w=283 m, R=.27 x $10^{-4}\Omega$ L=.15 x 10^{-7} Henries), for n=4 (dike-loop parameters: h=856 m, d=576 m, w=102 m, R=.94 x $10^{-5}\Omega$, L=.97 x 10^{-8} Henries) and for a Dike Depth of 300 m.

n = 1 and 207 Ω-m for n = 2 for the inversion at 10 Hz. The SE represents an average error in fit of less than 10% of the total "gull-wing" anomaly. The values of SE at 100 Hz are equally low. Similar results were obtained for the inversions at 1 Hz and 50 Hz.

The dike-loop parameters obtained in the inversion of the laboratory model data are summarized in Fig. 19 and Fig. 20. All five parameters exhibit a dispersion with frequency and dipole separation. 'h' decreases with decreasing dipole separation. In fact, as both the frequency and dipole separation decrease, 'h' approaches the actual value of the dike depth at 300 m in geophysical scale. 'h' also tends to increase with increasing frequency. Burying the loop deeper in the half-space achieves the same attenuation of the EM fields as that associated with the skin depth effect.

The parameter 'd' also increases with dipole separation. However, 'd' decreases with increasing frequency. Decreasing 'd' reduces the area of the loop. This, in turn, reduces the induced EMF in the loop, resulting in a reduced EM coupling anomaly consistent with the observed attenuations. In this way, 'd' is negatively correlated with 'h'.

As dipole separation and frequency are increased, the value of 'w' approaches the actual dike width of 100 m in geo-

GEOMETRIC "DIKE - LOOP" PARAMETERS

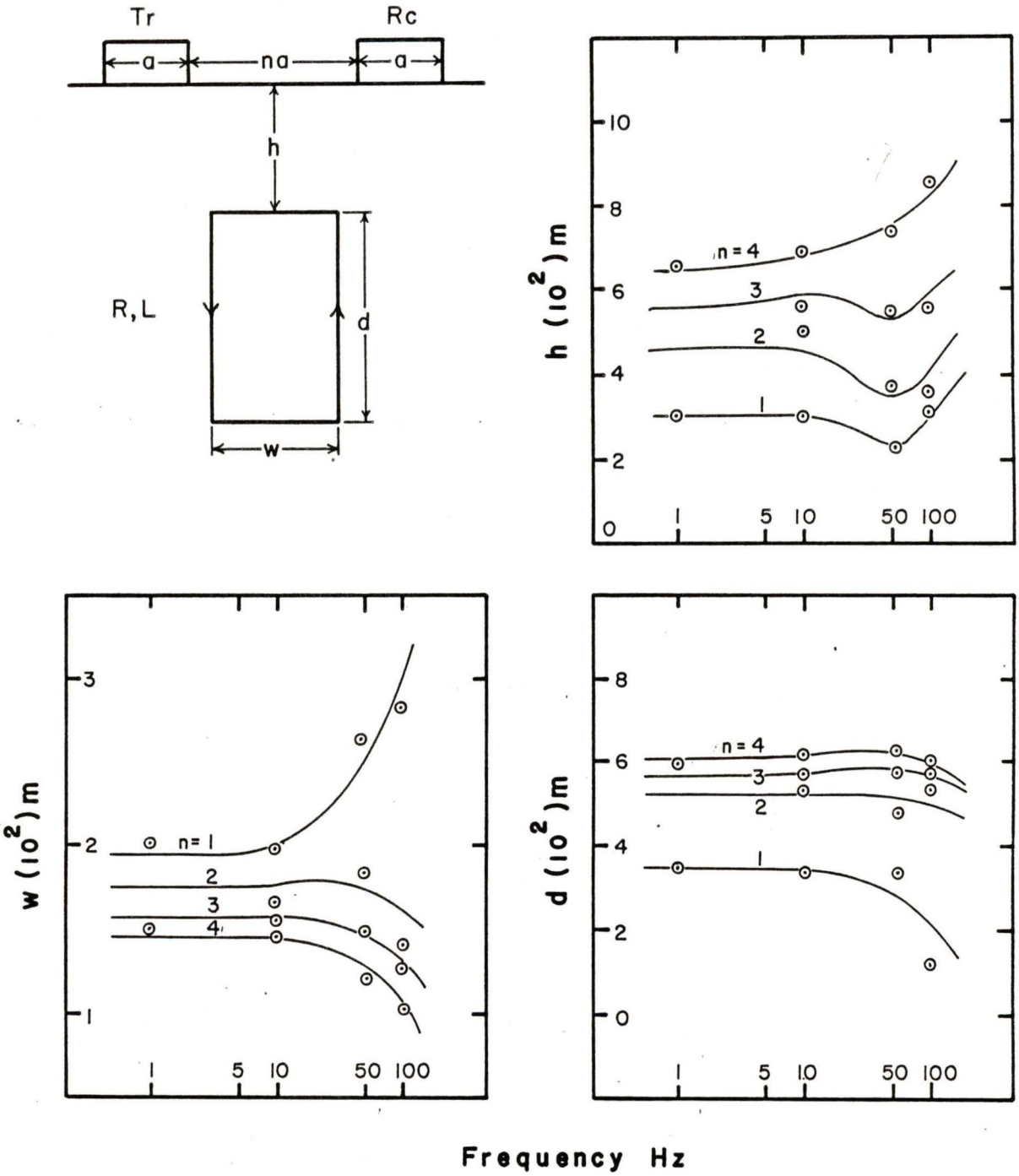

FIG. 19 Variation of the Geometric "Dike-Loop" Parameters ('h', 'd', 'w') with Frequency and Dipole Separation

ELECTRICAL "DIKE-LOOP" PARAMETERS

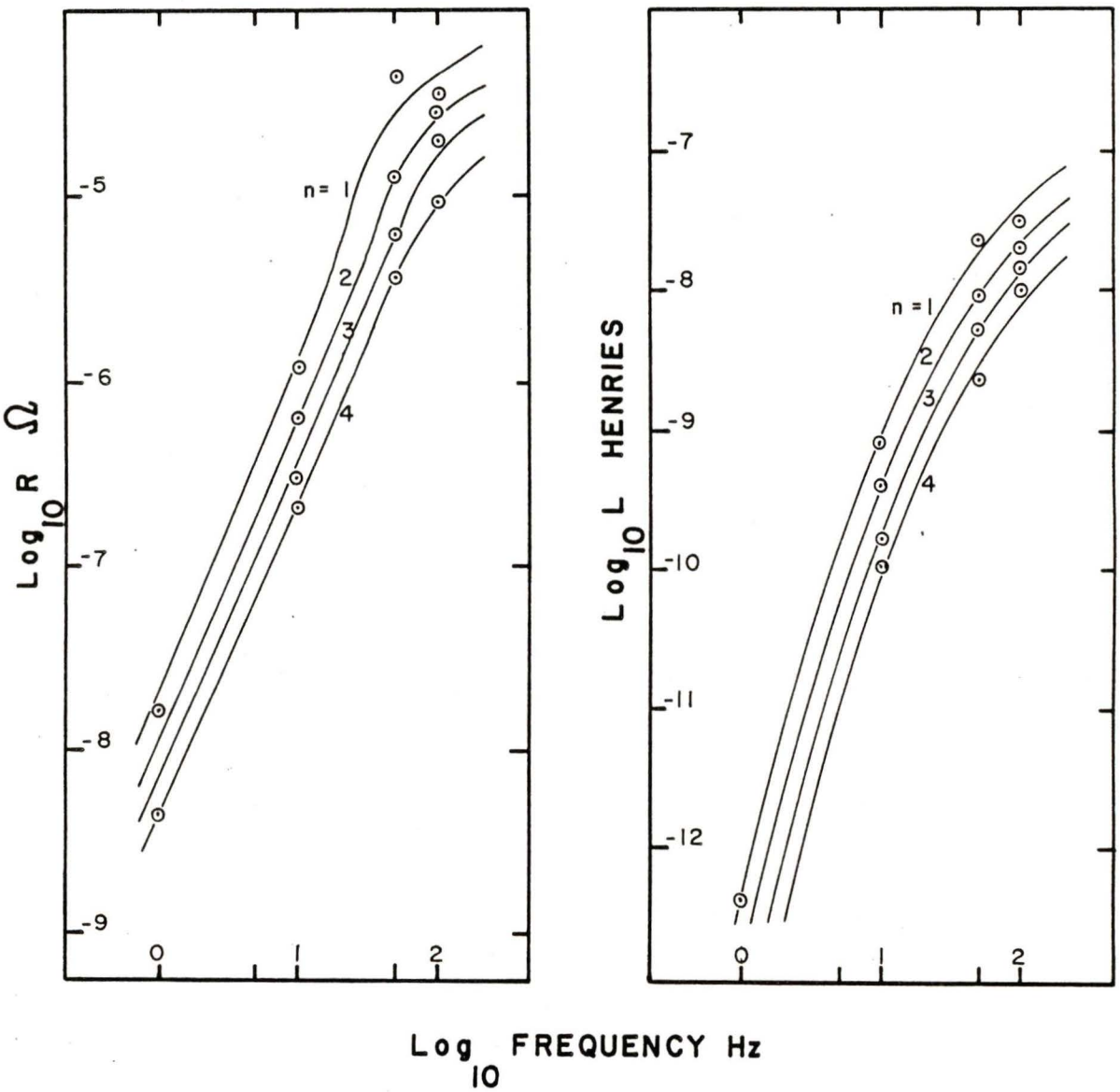

FIG. 20 Variation of the Electric "Dike-Loop" Parameters (R, L) with Frequency and Dipole Separation

physical scale. Therefore, in the field, more accurate estimates of dike width will be achieved using relatively large dipole separations and high frequencies.

In general, the frequency dependency of the geometric dike-loop parameters is weak. Conversely, the frequency dependency of the electrical dike-loop parameters is very strong, as expected. As illustrated in Fig. 20, both R and L vary with frequency over several orders of magnitude. Varying the dipole separation results in a parallel displacement of R and L on the LOG-LOG plots. This might correspond to a multiplicative change in the parameters that is constant with frequency. As was expected, L is 2 to 3 orders of magnitude smaller than R.

The DDL model was successfully used to describe the EM coupling effect along each individual traverse inverted. Unlike the empirical models dealt with in Chapter 4, this successful description included the region of positive phase over the dike. The variation of the dike-loop parameters with frequency is due primarily to the physical simplification of representing the dike by a conducting loop. The good agreement obtained between the DDL and laboratory model apparent resistivities along the individual traverses suggest that a different equivalent current loop exists for each configuration of the EM fields in the laboratory model.

6.3 Discussion

Although good agreement was obtained between the DDL model traverses and the laboratory model traverses, the agreement was not exact. This might be explained by experiemental error. As mentioned earlier, on each occasion when the distance between the electrodes is set, a mechanical error of $\pm$ .5 cm, or 10% of the dipole length, could occur. In the DDL calculation, 'a' was set at a constant value of 500 m geophysical scale. The DDL model also assumes that the contacts of the transmitter and receiver dipoles are points. In the laboratory model, the tips of the electrodes have a diameter of .5 cm in order to keep the current densities low. Hence, the laboratory measurements might be considered to be integrations of the DDL results over the net area of the laboratory electrode contacts. Other sources of error might be due to irregularities in the configuration of the laboratory model. The graphite dike might not have been exactly vertical, or the traverse might not have been exactly perpendicular to the strike of the dike. This latter error would significantly affect assumptions based on bi-lateral symmetry.

The weakness of the variation of the geometric dike-loop parameters with frequency suggests that these parameters might not truly vary with frequency and that the variation might be

due to other causes such as irregularities in the configuration of the laboratory model and inter-dependencies among the dike-loop parameters. The strong variation with frequency of the electrical dike-loop parameters suggests that this is a real response to variations of the EM properties of the dike with frequency. Hence, by fixing the geometric dike-loop parameters at their average values with frequency, inversions for apparent resistivities along traverses could be re-computed to obtain new values for R and L that might yield a closer match between the DDL model and the laboratory model.

As desired, the dike-loop parameters are constant with array position; unfortunately, they vary with frequency. Further work is required to develop a method of predicting this variation with frequency. When such a method is available, the DDL model will be even more successful at describing EM coupling for the embedded dike, and will facilitate more accurate removal of EM coupling from the spectral IP signal.

Several changes might be made in the DDL model which could improve its general usefulness and accuracy. The angle of inclination of the wire loop to the vertical might be included as a sixth parameter. By tilting the loop, the EM coupling effect for a dipping dike might be estimated. The rectangular loop might be replaced by an elliptical loop. 'w' and 'd'

would then describe the lengths of the major and minor axes of the loop. In nature, electrical currents do not turn at discontinuous corners; they flow in continuous curves. The single loop might also be replaced by a series of coplanar loops arranged so that the current density is larger near the top of the set of loops than near the bottom. This would achieve a more accurate representation of the eddy currents induced in the dike. Finally, a loop, or set of loops, might be introduced in the strike plane of the dike to account for EM coupling that would result if the traverse were not perpendicular to the strike of the dike.

6.4 Summary

Inversions of the laboratory model apparent resistivities were made using the dipole-dipole-loop (DDL) analytical model for traverses made at simulated frequencies of 1, 10, 50 and 100 Hz and for dipole separations of n = 1 to n = 4 and a single simulated dike depth of 300 m. As expected, the DDL apparent resistivity traverses displayed a "gull-wing" anomaly that was symmetrical about the origin over the centre of the loop. For a given set of dike-loop parameters, the DDL "gull-wing" anomaly decreased with increasing frequency and increased with increasing dipole separation. This was similar to the variations observed in the laboratory model traverses.

The inversions resulted in excellent agreement between the DDL model and laboratory model apparent resistivities. The standard error of fit computed for each inversion was typically less than 10% of the magnitude of the "gull-wing" anomaly. The dike-loop parameters resulting from the inversions demonstrated dispersions with frequency and dipole separation. The depth of the dike 'h' was determined by using low frequencies and short dipole separations. The width of the dike 'w' was determined by using high frequencies and long dipole separations. The depth extent 'd' of the loop varied from 100 m to 600 m in geophysical scale indicating that the eddy currents induced in the dike were concentrated within the top 1000 m of the dike, as was expected. The electrical dike-loop parameters (R and L) showed strong dispersion with frequency. L was consistently 2 to 3 orders of magnitude smaller than R, as expected.

The parameters of the DDL model are constant with array position, but vary with frequency. Further work is required to develop a method for predicting this variation with frequency to facilitate more accurate descriptions of EM coupling for the embedded dike, leading to a more accurate removal of EM coupling from the spectral IP signal for a naturally occurring dike.

Suggestions were made concerning ways to increase the accuracy and general applicability of the DDL model in modeling various configurations of ore bodies and dipole arrays.

CHAPTER 7

GENERAL SUMMARY AND CONCLUSIONS

The purpose of the work reported in this thesis was to study the response of EM coupling for the case of a vertical conducting dike embedded in a uniform poorly conducting host earth. A laboratory analogue scale model of the embedded dike was used that would provide spectral IP measurements comprised mainly of an EM coupling component. The conducting dike was simulated by a graphite plate, while the uniform host earth was simulated by a brine solution in a plywood tank. The laboratory model satisfied the electromagnetic scaling conditions derived from Maxwell's equations. Since the IP effect for the materials used in the laboratory model is negligible, it was concluded that the spectral IP measurements obtained from the model were due primarily to EM coupling between the dipole array and the conducting graphite and brine.

Spectral IP measurements were obtained along traverses over the laboratory model for simulated frequencies in the range .25 Hz to 512 Hz, for dipole separations of n = 1 to n = 4, and for simulated dike-depths of 300, 500 and 1000 m. All traverses were made in the region from Y = -50 cm to

Y = +50 cm in the tank, where edge effects were minimal. The spectral IP measurements along each traverse were normalized by setting the quadrature part to zero and the in-phase part to .3 volts at the reference location (Y = -50 cm) far from the influence of the dike. The normalization procedure removed the frequency response of the instruments. It also removed the frequency response of the uniform host earth. However, analysis of the complex impedance at the reference location indicated that the brine was an adequate simulation of a uniform poorly conducting host earth.

The normalized spectral IP measurements displayed the typical "gull-wing" character of the EM response of a naturally occurring conducting dike. The magnitude of this anomaly decreased with increasing frequency in response to the skin depth effect, and increased with increasing dipole separation. By treating a change in the transmitter current as a multiplicative gain, and by treating the normalization procedure as a linear scaling, the model normalized measurements were used to obtain apparent resistivities that were characteristic of both the uniform host earth and the embedded dike.

The laboratory model apparent resistivities were inverted, using the Marquardt algorithm, for two empirical models of EM coupling based on the Cole-Cole dispersion. The Cole-Cole

dispersion was not a suitable model of EM coupling for the embedded dike since it yields an apparent resistivity with a phase that is consistently small and negative. The apparent resistivities for the laboratory model display positive phases in the region over the dike. Inversions were made of laboratory model spectra collected at 12 stations along the traverse (Y = -50, -40 --- -20, -17.5, -15 --- 0 cm) using a generalized Cole-Cole dispersion and the product of two generalized Cole-Cole dispersions. These inversion calculations broke down in the region of positive phase over the dike. However, good fits were obtained in the regions far from the dike. It was concluded that the Cole-Cole dispersion and its derivatives were not suited to describing EM coupling for an embedded body of finite dimensions, but were better suited to describing EM coupling for a uniform conducting earth.

An analytical model of EM coupling for a conducting dike embedded in a poorly conducting uniform host earth was developed, and is referred to as the dipole-dipole-loop (DDL) model. In the DDL model, the dike is replaced by a thin conducting loop coplanar with the array dipoles. EM coupling for this model was derived using the principles of EM induction. All linear current elements were treated as strings of point electric dipoles. The expressions for the EM fields of point

electric dipoles on the surface of, or embedded in, a uniform conducting half-space are well known. An expression for the apparent resistivity of the DDL model was developed. This expression has three independent variables (frequency, array position and dipole separation) and five descriptive parameters (loop depth, width and depth extent, and the loop resistance and self inductance).

The apparent resistivities from the DDL model also display a "gull-wing" anomaly that is symmetrical about the origin above the centre of the loop. This anomaly decreases with increasing frequency and increases with increasing dipole separations. Inversions were made of the laboratory model apparent resistivities using the DDL model for values along traverses at 1, 10, 50 and 100 Hz for dipole separations of n = 1 to n = 4 at a single simulated dike depth of 300 m. Excellent agreement was obtained between the DDL and laboratory model apparent resistivities along each traverse inverted. The standard error of fit calculated for each inverted traverse was less than 10% of the magnitude of the "gull-wing" anomaly.

The dike-loop parameters obtained from these inversions displayed dispersions with dipole separation and frequency. These dispersions are due primarily to the physical simplification of representing the conducting dike by a conducting loop.

The inversion results showed that an equivalent current loop could be obtained for each electromagnetic configuration of the dike and dipole array. In this manner, the DDL model, unlike the empirical models, is successful in describing EM coupling over the entire traverse, including the region of positive phase over the dike.

It was found that the value of the loop depth approached the value of the true dike depth at low frequencies and small dipole separations. Conversely, the value of the loop width approached the value of the true dike width at high frequencies and large dipole separations. Knowledge of these dimensions is important to exploration geophysicists.

The dike-loop parameters are constant with array position, but vary with frequency. Further work is required before it can be predicted how these parameters will vary with frequency in the case of an embedded dike. When this is achieved, the DDL model will provide even more accurate descriptions of EM coupling for the embedded dike and might facilitate more precise removal of the EM coupling component from the spectral IP signal. It might be, however, that making a single inversion with the entire data set, as a function of frequency, array position and dipole separation, using the DDL model would result in a single set of dike-loop parameters that would

account for the major portion of the EM coupling component of the spectral IP signal. This remains to be tested with the laboratory model apparent resistivities.

Once a DDL model has been developed in which the frequency dependence of its parameters is well understood, attempts might be made to remove the EM coupling component from spectral IP measurements containing both EM coupling and IP components. This might be achieved by adding to the DDL model an expression that describes the IP effect and using the combined expression to describe the complete spectral IP signal. A data set on which to test this expression could be obtained by adding an artificial IP response to the laboratory dike model apparent resistivities. The combined DDL - IP expression might then be used to invert this data set, thus separating the two signal components. If the laboratory model apparent resistivities are successfully retrieved in this manner, inversions might then be made of spectral IP measurements of a well delineated, naturally occurring conducting dike. Once successful interpretations of the resulting DDL and IP parameters have been made in such a case, the combined DDL - IP expression could be applied in mineral and petroleum exploration.

REFERENCES

Anderson, W. L. 1977. Marquardt inversion of vertical magnetic field measurements from a grounded wire source. U. S. Geological Survey, USGS-G9-77-06.

Banos, A., Jr. 1966. Dipole Radiation in the Presence of a Conducting Half-Space. Pergamon Press.

Best, M. E. 1983. Research Scientist, Shell Canada Ltd. Personal communication.

Bleil, D. F. 1953. Induced polarization: a method of geophysical prospecting. Geophysics, 18(3), 636-662.

Brant, A. A. 1959. Historical summary of overvoltage developments by Newmont Exploration Limited, 1946-1955. In: Overvoltage Research and Geophysical Applications. J. R. Wait, ed. Pergamon Press, 1-3.

Dey, A. and Morrison, H. F. 1973. Electromagnetic coupling in frequency and time domain induced polarization surveys over a multilayered earth. Geophysics, 38, No. 2, 380.

Dosso, H. W. 1966a. A plane-wave analogue model for studying electromagnetic variations. Can. J. Phys., 44, 67-80.

Dosso, H. W. 1973. A review of analogue model studies for the coast effect. Phys. Earth Planet Int., 7, 297-302.

Frischknecht, F. C. 1971. Electromagnetic scale modelling. In: Electromagnetic Probing in Geophysics. J. R. Wait, ed. Galem Press.

Grant, F. S. and West, G. F. 1965. Interpretation Theory in Applied Geophysics. McGraw-Hill Book Company.

Hallof, P. G. 1965. The proper choice of frequencies for induced polarization measurements. Presented at the 35th Annual International SEG Meeting.

Hallof, P. G. 1973. The IP phase measurement and inductive coupling. Geophysics. 38, No. 6, 1202.

Hohmann, G. W. 1971. Electromagnetic scattering by conductors in the earth near a line source of current. Geophysics, 36, No. 1, 101.

Hohmann, G. W. 1973. Electromagnetic coupling between grounded wires at the surface of a two layer earth. Geophysics, 38, No. 5, 854.

Klein, J. D. 1983. Spectral induced polarization survey, David Field, Alberta, Presented at the annual technical conference of the C.S.E.G., Calgary, Alberta.

Madden, T. R. and Cantwell, T. 1967. Induced polarization, a review. In: Mining Geophysics. Vol. II, S.E.G., 373-400.

Madden, T. R. and Marshall, D. J. 1958. A laboratory investigation of induced polarization. U. S. A. E. C. Rep., RME-3156.

Madden, T. R. and Marshall, D. J. 1959a. Induced polarization, a study of its causes. Geophysics, 24, 790-816.

Madden, T. R. and Marshall, D. J. 1959b. Electrode and membrane polarization. U.S.A.E.C. Rep., RME-3157.

Marquardt, D. W. 1963. An algorithm for least-squares estimation of non-linear parameters. J. Soc., Indust. Appl. Math., 11, No. 2, 431-441.

Millet, F. B., Jr. 1967. Electromagnetic coupling of colinear dipoles on a uniform half-space. In: Mining Geophysics. Vol. II, SEG.

Naidu, P. 1966. Theoretical analyses of apparent resistivity over a dike of arbitrary shape. Geophysical Prospecting, XIV, 168-183.

Ness, N. 1963. Em coupling of finite colinear dipoles over a two-layered half-space. N. Ness Condulting Reports.

Pelton, W. H. 1977. Interpretation of induced polarization and resistivity data. Ph.D. dissertation, University of Utah.

Pelton, W. H., Ward, S. H., Hallof, P. G., Sill, W. R., Nelson, P. H. 1978. Mineral discrimination and removal of inductive coupling with multifrequency IP. Geophysics, 43, 588-609.

Ramaswamy, V. 1973. Electromagnetic fields of a horizontal magnetic dipole situated above and within a two-layer earth. Ph.D. dissertation, University of Victoria.

Ramaswamy, V., Dosso, H. W. 1978. Analogue model measurements for a horizontal magnetic dipole embedded within a conducting medium. Phys. Earth Planet. Inter., 17, 295-299.

Schlumberger, C. 1920. Étude sur la prospection electrique du sous-sol. Gauthier-Villars.

Seigal, H. O. 1959. Mathematical formulation and type curves for induced polarization. Geophysics, 25, 547-565.

Strangeway, D. W. 1966. Electromagnetic scale modelling. In: Methods and Techniques in Geophysics. S. K. Runcorn, ed., Interscience Publishers.

Sumner, J. S. 1976. Principles of Induced Polarization for Geophysical Exploration. Elsevier Scientific Publishing Company.

Sunde, E. D. 1949. Earth Conduction Effects in Transmission Systems. Van Norstrand.

Telford, W. M., Geldart, L. P., Sheriff, R. E., Keys, D. A. 1981. Applied Geophysics. Cambridge University Press.

Wait, J. R. 1953. The fields of a line source of current over a stratified conductor. Appl. Sci. Res. Sec. B, 4-5, 279.

Wait, J. R. 1959 (ed.) Overvoltage Research and Geophysical Applications. Pergamon Press.

Wait, J. R. 1966. Fields of a horizontal dipole over a stratified anisotropic half-space. IEEE Trans. on Ant. and Prop., AP-14, 790.

Wait, J. R. 1970. Electromagnetic Waves in Stratified Media. Pergamon Press.

Wait, J. R. 1971 (ed.) Electromagnetic Probing in Geophysics. Golem Press.

Wait, J. R. 1983. Geo-electromagnetism. Academic Press.

Weaver, J. T. 1967. The quasi-static field of an electric dipole embedded in a two-layer conducting half-space. Canadian Journal of Physics, 45, 1981-2002.

Weidelt, P. 1983. The harmonic and transient electromagnetic response of a thin dipping dike. Geophysics, 48, 934-952.

Wynn, J. 1974. Electromagnetic coupling in induced polarization. Ph.D. dissertation, University of Arizona.

Zonge, K. 1972. Electrical properties of rocks as applied to geophysical prospecting. Ph.D. dissertation, University of Arizona.

APPENDIX I

COMPUTER PROGRAMME FOR COMPLEX IMPEDANCE OF A UNIFORM EARTH

Presented here is a copy of the computer programme used to compute the complex impedances and apparent resistivities of an in-line dipole-dipole array coupled to a uniform conducting earth as functions of frequency and dipole separation. The expressions used in this programme were derived from Sunde's (1949) expressions for the complex impedance between two wires lying on the surface of a conducting half-space in an arbitrary configuration.

```
C      **********      HEC      **********
C
C
C  THIS PROGRAMME COMPUTES THE COMPLEX IMPEDANCE BETWEEN TWO
C  COLINEAR DIPOLES SITUATED OVER A HOMOGENEOUS HALF SPACE.
C
C  PARAMETERS
C                W(22)=ANGULAR FREQUENCY IN TRANSMITTING DIPOLE.
C                A    =DIPOLE LENGTH.
C                N    =INTEGRAL DIPOLE SPACINGS OF 'A'.
C                P    =DC RESISTIVITY OF HOMOGENEOUS HALF SPACE.
C                ZP(22,4)=COMPLEX IMPEDANCE ARRAY.
C                ZA(22,4)=AMPLITUDE OF ZP(22,4)
C                ZPH(22,4)=PHASE OF ZP(22,4)
C                ZR(22,4)=APPARENT RESISTIVITY
C
C  DIMENSIONS:
C
      REAL W(22),F(22),A,P,AMP,ZA(22,4),ZPH(22,4),R,Q
      COMPLEX ZP(22,4),K(22),DI,ZR(22,4)
C
C  INPUT DATA:
C
      READ(1,100) (F(I),I=1,22)
      READ(1,101) M,A,P
100   FORMAT(E8.3)
101   FORMAT(I2,F4.2,E13.5)
      WRITE(6,115) (F(I),I=1,22)
115   FORMAT(' ',E8.3)
      WRITE(6,116) M,A,P
116   FORMAT(' ',I2,1X,F4.2,E13.5)
C
C  BEGIN COMPUTATION OF HEC IMPEDANCES:
C
      PI=ABS(ARCOS(-1.))
      WRITE(6,50) PI
50    FORMAT(' ','PI=',E13.5)
      U=4.*PI/(1.E7)
C
      DO 102 I=1,22
       W(I)=2.*PI*F(I)
       K(I)=CSQRT((0.,1.)*U*W(I)/P)
       DO 103 N=1,M
        CALL SIMP(N,A,K(I),DI)
        ZP(I,N)=P/(2.*PI*N*(N+1)*(N+2)*A)
     1           -P*(2.*CEXP(-K(I)*(N+1)*A)/((N+1)*A)
     2           -CEXP(-K(I)*(N+2)*A)/((N+2)*A)
     3           -CEXP(-K(I)*N*A)/(N*A))/(4.*PI)
     4           -P*DI*(K(I)**2)/(4.*PI)
103    CONTINUE
102   CONTINUE
C
C
C  CONVERT IMPEDENCES TO APPARENT RESISTIVITIES.
C
```

```
      DO 110 I=1,22
       DO 111 J=1,M
          ZR(I,J)=PI*J*(J+1)*(J+2)*A*ZP(I,J)
111    CONTINUE
110   CONTINUE
C
CCC
C  CONVERT REAL AND QUADRATURE PARTS TO AMPLITUDE AND PHASE
C
      DO 40 I=1,22
       DO 60 J=1,M
        R=REAL(ZR(I,J))
        Q=AIMAG(ZR(I,J))
        ZA(I,J)=CABS(ZR(I,J))
        ZPH(I,J)=ATAN2(Q,R)
60     CONTINUE
40    CONTINUE
C
CCC
C  OUTPUT BOTH THE NORMALIZED AND THE UN-NORMALIZED IMPEDANCE
C  ARRAYS
C
      WRITE(2,112)
112   FORMAT('0','      ***** HOMOGENEOUS EARTH : COL.DIP.RESIST, **
      DO 113 N=1,M
       WRITE(2,106) N
106    FORMAT('0','N=',I1)
       WRITE(2,108) (F(I),ZA(I,N),ZPH(I,N),I=1,22)
108    FORMAT(' ',E10.3,2E15.5)
113   CONTINUE
      STOP
      END
C
CCCCCCCC
C
      **********      SUBROUTINE SIMP      **********
C
      SUBROUTINE SIMP(NS,AS,KS,DIS)
C
CCCCCCCCC
C  THIS SUBROUTINE USES A COMBINATION OF SIMPSONS RULE AND
C  NEWTON'S 3/8 RULE TO COMPUTE THE DOUBLE INTEGRAL:
C
      DIS=I(0,A).I( N+1 A-X, N+2 A-X).CEXP(-KY)/Y.DY.DX
C
CCCCCCCCC
C  EQUIDISTANT QUADRATURE WITH 20 INTEVALS IS USED,
C  (IE. IF A=5CM, ERROR=(5/20)**5=1.E-4CM)
C
CCCCCCCCC
C  DIMENSIONS:
C
      REAL X(21),Y(21),FRX(21),FQX(21),GRY(21),GQY(21),Z(21)
      REAL A,R,Q
      COMPLEX KS,DIS
```

```
C
      R=REAL(KS)
      Q=AIMAG(KS)
C
C  COMPUTE X ARRAY:
C
      HX=(AS-0.)/20.
      DO 201 I=1,21
       X(I)=0.+(I-1)*HX
201   CONTINUE
C
C  PERFORM INNER INTEGRATION OVER Y:
C
      DO 202 I=1,21
       Y1=(NS+1)*AS-X(I)
       Y2=(NS+2)*AS-X(I)
       HY=ABS(Y2-Y1)/20.
       DO 203 J=1,21
        Y(J)=Y1+(J-1)*HY
        GRY(J)=EXP(-R*Y(J))*COS(Q*Y(J))/Y(J)
        GQY(J)=EXP(-R*Y(J))*SIN(Q*Y(J))/Y(J)
203    CONTINUE
       CALL QSF(HY,GRY,Z,21)
       FRX(I)=Z(21)
       CALL QSF(HY,GQY,Z,21)
       FQX(I)=Z(21)
202   CONTINUE
C
C  PERFORM OUTER INTEGRATION OVER X:
C
      CALL QSF(HX,FRX,Z,21)
      DR=Z(21)
      CALL QSF(HX,FQX,Z,21)
      DQ=-Z(21)
      DIS=DR+(0.,1.)*DQ
C
C  RETURN DOUBLE INTEGRAL VALUE 'DIS'
C
      RETURN
      END
C
CCCCCCC
CCC
CCC     **********     SUBROUTINE QSF     **********
CCC
C
      SUBROUTINE QSF(H,T,Z,NDIM)
C
C  PURPOSE: TO COMPUTE THE VECTOR OF INTEGRAL VALUES FOR A GIVEN
C  EQUIDISTANT TABLE OF FUNCTION VALUES.
C
C  PARAMETERS:
C            H=INCREMENT OF ARGUEMENT VALUES.
```

```
C              T=INPUT VECTOR OF THE FUNCTION.
CC             Z=OUTPUT VECTOR OF INTEGRAL VALUES.
CC             NDIM=NUMBER OF POINTS IN THE QUADRATURE
CC                  (IE. NDIM=NUMBER OF INTERVALS +1 )
CC
C  REMARKS: NO ACTION IF NDIM < 3.
C  METHOD: BEGINNING WITH Z(1)=0. , EVALUATION OF VECTOR Z(2) IS
C  DONE BY MEANS OF A SIMPSON'S RULE OR A NEWTON'S 3/8 RULE OR A
C  COMBINATION OF BOTH. TRUNCATION ERROR IS OF THE ORDER OF H**5,
C  IF NDIM=3 , TRUNCATION ERROR IS OF THE ORDER OF H**4.
CC
C  REFERENCE: HILDEBRAND , INTRO TO NUMERICAL ANALYSIS , PG 71-76.
C
C  TEXT
C
      DIMENSION T(1),Z(1)
      HT=.3333333*H
      IF(NDIM-5) 7,8,1
C
C  NDIM > 5 ; PREPARE FOR INTEGRATION LOOP.
C
1     SUM1=T(2)+T(2)
      SUM1=SUM1+SUM1
      SUM1=HT*(T(1)+SUM1+T(3))
      AUX1=T(4)+T(4)
      AUX1=AUX1+AUX1
      AUX1=SUM1+HT*(T(3)+AUX1+T(5))
      AUX2=HT*(T(1)+3.875*(T(2)+T(5))+2.625*(T(3)+T(4))+T(6))
      SUM2=T(5)+T(5)
      SUM2=SUM2+SUM2
      SUM2=AUX2-HT*(T(4)+SUM2+T(6))
      Z(1)=0.
      AUX=T3+T3
      AUX=AUX+AUX
      Z(2)=SUM2-HT*(T(2)+AUX+T(4))
      Z(3)=SUM1
      Z(4)=SUM2
      IF(NDIM-6) 5,5,2
C
C  INTEGRATION LOOP
C
2     DO 4 I=7,NDIM,2
      SUM1=AUX1
      SUM2=AUX2
      AUX1=T(I-1)+T(I-1)
      AUX1=AUX1+AUX1
      AUX1=SUM1+HT*(T(I-2)+AUX1+T(I))
      Z(I-2)=SUM1
      IF(I-NDIM) 3,6,6
3     AUX2=T(I)+T(I)
      AUX2=AUX2+AUX2
      AUX2=SUM2+HT*(T(I-1)+AUX2+T(I+1))
4     Z(I-1)=SUM2
5     Z(NDIM-1)=AUX1
      Z(NDIM)=AUX2
```

```
      RETURN
6     Z(NDIM-1)=SUM2
      Z(NDIM)=AUX1
      RETURN
C
C  END INTEGRATION LOOP
C
7     IF(NDIM-3) 12,11,8
C
C  NDIM=4OR5
C
8     SUM2=1.125*HT*(T(1)+3*T(2)+3*T(3)+T(4))
      SUM1=T(2)+T(2)
      SUM1=SUM1+SUM1
      SUM1=HT*(T(1)+SUM1+T(3))
      Z(1)=0.
      AUX1=T(3)+T(3)
      AUX1=AUX1+AUX1
      Z(2)=SUM2-HT*(T(2)+AUX1+T(4))
      IF(NDIM-5) 10,9,8
9     AUX1=T(4)+T(4)
      AUX1=AUX1+AUX1
      Z(5)=SUM1+HT*(T(3)+AUX1+T(5))
10    Z(3)=SUM1
      Z(4)=SUM2
      RETURN
C
C  NDIM=3
C
11    SUM1=HT*(1.25*T(1)+2.*T(2)-.25*T(3))
      SUM2=T(2)+T(2)
      SUM2=SUM2+SUM2
      Z(3)=HT*(T(1)+SUM2+T(3))
      Z(1)=0.
      Z(2)=SUM1
12    RETURN
      END
C
C
C
C  ******** NOTE: QSF IS A COMMERCIAL SUBROUTINE. ********
C
C                          END
```

APPENDIX II

(a) THE ELECTRIC FIELD OF A POINT ELECTRIC DIPOLE ON THE SURFACE OF A CONDUCTING HALF-SPACE

In this appendix, the electric field of a point electric dipole on the surface of a conducting half-space is given for the case of a sub-surface field point. Ward (1967) shows that the Hertz vector potential of a point dipole on the surface of a conducting half-space has the components:

$$\pi_x = \frac{(I\,ds)\,j\omega\mu_0}{2\pi k^4}\left(\frac{\partial^2 P}{\partial z^2} - k^2\frac{\partial N}{\partial z} + \frac{\partial^3 N}{\partial z^3}\right), \qquad \text{(a-1)}$$

$$\pi_z = \frac{(I\,ds)\,j\omega\mu_0}{2\pi k^4}\left(\frac{\partial^2 P}{\partial x \partial z} + \frac{\partial^3 N}{\partial x \partial z^2}\right), \qquad \text{(a-2)}$$

where

$$P = \frac{e^{-kR}}{R}, \quad R = \sqrt{x^2+y^2+z^2}, \qquad \text{(a-3)}$$

and

$$N = I_0\left(\tfrac{k}{2}(r-z)\right) K_0\left(\tfrac{k}{2}(r+z)\right), \qquad \text{(a-4)}$$

and I_0 and K_0 are modified Bessel functions of the first and second kind respectively. The electric field radiated by the point dipole can be expressed in terms of the Hertz vector potential as

$$\underset{\sim}{E} = \nabla\left(\nabla\cdot\underset{\sim}{\pi}\right) + k^2\underset{\sim}{\pi}\,. \qquad \text{(a-5)}$$

So, $$E_x = \frac{\partial}{\partial x}\left(\frac{\partial \pi_x}{\partial x} + \frac{\partial \pi_z}{\partial z}\right) + k^2 \pi_x \qquad \text{(a-6)}$$

and $$E_z = \frac{\partial}{\partial z}\left(\frac{\partial \pi_x}{\partial x} + \frac{\partial \pi_z}{\partial z}\right) + k^2 \pi_z \qquad \text{(a-7)}$$

Using (a-1) and (a-2) in (a-6) and (a-7) gives after simple algebra,

$$E_x = -\frac{(Ids)\, j\omega\mu_0}{2\pi k^4}\left(\frac{\partial^2 P}{\partial z^2} - \frac{\partial^3 N}{\partial y^2 \partial z}\right), \qquad \text{(a-8)}$$

and $$E_z = \frac{(Ids)\, j\omega\mu_0}{2\pi k^4}\left(\frac{\partial^2 P}{\partial x \partial z}\right). \qquad \text{(a-9)}$$

Using equations (a-3) and (a-4) in (a-8) and (a-9) yields after long algebra,

$$E_z = \frac{(Ids)\, j\omega\mu_0}{2\pi k^2} \cdot \frac{zx}{R^5}\left(3 + 3kR + k^2R^2\right) e^{-kR}, \qquad \text{(a-10)}$$

and

$$E_x = \frac{(Ids)\, j\omega\mu_0}{2\pi k^2}\left\{\left(\frac{k}{R^2} + \frac{1}{R^3} - z^2\left(\frac{k^2}{R^3} + 3\frac{k}{R^4} + \frac{3}{R^5}\right)\right) e^{-kR}\right.$$

$$+ I_0(a)\, K_0(b)\left(\frac{k}{2}\right)^2\left(\frac{xz}{R^2}\right)$$
$$+ I_0(a)\, K_1(b)\left(\frac{k}{2}\right)\left(\frac{xz}{R^3}\right)$$
$$+ I_0(a)\, K_2(b)\left(\frac{k}{2}\right)^2\left(\frac{xz}{2R} + \frac{1}{2R}\right)$$
$$+ -I_1(a)\, K_0(b)\left(\frac{k}{2}\right)\left(\frac{xz}{R^3}\right)$$
$$+ -I_1(a)\, K_1(b)\left(\frac{k}{2}\right)^2\left(\frac{2xz}{R^2}\right)$$
$$\left. + I_2(a)\, K_0(b)\left(k/2\right)^2\left(\frac{xz}{2R^2} - \frac{1}{2R}\right)\right\} \qquad \text{(a-11)}$$

where $$R = \sqrt{x^2 + z^2} \quad ,$$

$$a = \frac{k}{2}(R - z) \quad ,$$

$$b = \frac{k}{2}(R + z) \quad ,$$

$$k^2 = j\omega\mu_0\sigma \quad .$$

and

The expressions for $\mathcal{E}_{Tx}$ and $\mathcal{E}_{Tz}$ as defined in Chapter 5 are thus

$$\mathcal{E}_{Tx} = \frac{E_x}{I\,ds} \quad , \tag{a-12}$$

and

$$\mathcal{E}_{Tz} = \frac{E_z}{I\,ds} \quad . \tag{a-13}$$

APPENDIX II

(b) THE ELECTRIC FIELD OF AN EMBEDDED VERTICAL POINT ELECTRIC DIPOLE IN A CONDUCTING HALF-SPACE

In this appendix, the x component of the electric field of a vertical point electric dipole embedded in a uniform conducting earth to a depth 'h' is computed for a field point at surface. Weaver (1967) shows that the radial component of $\underset{\sim}{E}$ for cylindrical coordinates is

$$E_r' = F_2(r_0', \delta \sin 2\psi_0) - F_2(R_0', \delta \sin 2\bar{\psi}_0) , \qquad \text{(b-1)}$$

where $$E_r' = \frac{4\pi E_r}{(Ids)\mu_0\omega(\mu_0\sigma\omega)^{1/2}} ,$$

$$F_2(\rho, \chi) = \tfrac{1}{2}\chi(3 + 3\rho\sqrt{j} + j\rho^2)e^{-\rho\sqrt{j}} ,$$

$$r_0' = \alpha r_0 = \alpha\sqrt{r^2 + (z-h)^2} ,$$

$$R_0' = \alpha R_0 = \alpha\sqrt{r^2 + (z+h)^2} ,$$

$$\psi_0 = \cot^{-1}\left(\frac{z-h}{r}\right) , \quad \bar{\psi}_0 = \cot^{-1}\left(\frac{z+h}{r}\right),$$

and $$\alpha^2 = \mu\omega\sigma, \text{ and } r = \sqrt{x^2 + z^2} . \qquad \text{(b-2)}$$

The time dependency in Weaver's development is $e^{j\omega t}$; so

$$k^2 = j\omega\mu_0\sigma = j\alpha^2 . \qquad \text{(b-3)}$$

For field points in the $x-z$ plane,

$$E_r(r,z) = E_x(x,z) \quad . \tag{b-4}$$

Thus,

$$r_o = \sqrt{x^2 + (z-h)^2} \quad , \tag{b-5}$$

and

$$R_o = \sqrt{x^2 + (z+h)^2} \quad . \tag{b-6}$$

Substituting equations (b-2) into equation (b-1) yields after short algebra (and letting $z \to 0$)

$$E_x(R) = -\frac{j\omega\mu_o(Ids)}{2\pi k^2} \cdot \frac{xh}{R^5} (3+3kR+k^2R^2)e^{-kR} \quad , \tag{b-7}$$

where $R = (x^2+h^2)^{\frac{1}{2}}$

Notice that for $z=h$, equations (b-7) and (a-10) are identical in form but apposite in sign. For $\mathcal{E}_{vx}$ referred to in Chapter 5,

$$\mathcal{E}_{vx} = \frac{E_x(R)}{Ids} \quad . \tag{b-8}$$

Hence

$$\mathcal{E}_{Tz} = -\mathcal{E}_{vx} \quad .$$

APPENDIX II

(c) THE ELECTRIC FIELD OF AN EMBEDDED HORIZONTAL POINT ELECTRIC DIPOLE IN A CONDUCTING HALF-SPACE

In this appendix, the x component of the electric field of a horizontal point electric dipole embedded to a depth 'h' in a uniform conducting earth is computed for a field point at surface. Wait (1961) gives this component of the electric field as

$$E_x = \frac{(Id_s)\,\jmath\omega\mu_0}{4\pi K^2}\left[\left(\frac{\partial^2}{\partial x^2} - K^2\right)\left(P(R_0) - P(R_1)\right) - 2\left(\frac{\partial^2 P(R_1)}{\partial z^2} - \frac{\partial^3 N}{\partial y^2 \partial z}\right)\right], \qquad \text{(c-1)}$$

where

$$P(R) = \frac{e^{-KR}}{R}, \qquad \text{(c-2)}$$

$$R_0 = \sqrt{x^2 + y^2 + (z-h)^2},$$

$$R_1 = \sqrt{x^2 + y^2 + (z+h)^2},$$

and

$$N = I_0\left(\frac{K}{2}\left(R_1 - (z+h)\right)\right) K_0\left(\frac{K}{2}\left(R_1 + (z+h)\right)\right), \qquad \text{(c-3)}$$

and I_o and K_o are modified Bessel functions of the first and second kind respectively. After substituting for P and N and letting $z \to 0$, long algebra yields

$$E_x(x,0,0) = \frac{(Ids)\,j\omega\mu_o}{4\pi K^2}\left\{\frac{2Ke^{-KR}}{R^2} + \frac{2e^{-KR}}{R^3}\right.$$

$$-2h^2\left(\frac{K^2e^{-KR}}{R^3} + \frac{3Ke^{-KR}}{R^4} + \frac{3e^{-KR}}{R^5}\right)$$

$$+2\left(I_o(a)K_o(b)\left(\frac{K}{2}\right)^2\left(\frac{h}{R^2}\right)\right.$$
$$+I_o(a)K_1(b)\left(\frac{K}{2}\right)\left(\frac{h}{R^3}\right)$$
$$+I_o(a)K_2(b)\left(\frac{K}{2}\right)^2\left(\frac{h}{2R^2}+\frac{1}{2R}\right)$$
$$+I_1(a)K_o(b)\left(\frac{K}{2}\right)\left(\frac{h}{R^3}\right)$$
$$+I_1(a)K_1(b)\left(\frac{K}{2}\right)^2\left(\frac{2h}{R^2}\right)$$
$$\left.\left.+I_2(a)K_o(b)\left(\frac{K}{2}\right)^2\left(\frac{h}{2R^2}-\frac{1}{2R}\right)\right)\right\}, \qquad \text{(c-4)}$$

where
$$R = \sqrt{x^2+h^2},$$
$$a = \frac{K}{2}(R-h),$$
$$b = \frac{K}{2}(R+h),$$
and
$$K^2 = j\omega\mu_o\sigma.$$

For $\mathcal{E}_{HX}$ referred to in Chapter 5,

$$\mathcal{E}_{HX} = \frac{E_x(x,0,0)}{I\,ds}. \qquad \text{(c-5)}$$

Note that

$$\mathcal{E}_{HX} = \mathcal{E}_{TX}.$$

VITA

Surname: CHARTERS Given Names: ROBERT ANTHONY

Place of Birth: Calgary, Alberta. Date of Birth: September 23, 1959

Educational Institutions Attended:

UNIVERSITY OF VICTORIA 1977 - 1984

Degrees, Diplomas, Etc., Awarded:

B.Sc.	1982	University of Victoria
M.Sc. (anticipated)	1984	University of Victoria

Honours and Awards:

Prov. of British Columbia Grade 12 Scholarship	1977/78	
President's Entrance Scholarship	1977/78	University of Victoria
Woods Trust Scholarship	1980/81	University of Victoria
The Frank and Margaret Gibbs Scholarship	1981/82	University of Victoria
The Molson Companies Scholarship	1981/82	University of Victoria
Eligible for President's Scholarship, but could not accept due to awards already held	1980/81 1981/82	University of Victoria
The R. M. Pearce Memorial Fellowship	1982/83	University of Victoria

Honours and Awards:

N.S.E.R.C. Post-Graduate Scholarship	1982/83 1983/84	University of Victoria

Papers Presented at Scientific Meetings:

Charters, R. A., Dosso, H. W., Best, M. E. 1984. An Analogue Model Study of EM Coupling in Spectral IP Measurements for the Case of a Conducting Dike. Joint National Convention of the CSEG and CSPG at Calgary, Alberta.

PARTIAL COPYRIGHT LICENSE

I hereby grant the right to lend my thesis (the title of which is shown below) to users of the University Library, and to make single copies only for such users or in response to a request from the library of any other university, or similar institution, on its behalf or for any of its users. I further agree that permission for extensive copying of this thesis for scholarly purposes may be granted by me or a member of the University designated by me. It is understood that copying or publication of this thesis for financial gain shall not be allowed without my written permission.

Title of Thesis:

ELECTROMAGNETIC IP RESPONSE OF A
CONDUCTING DIKE IN A CONDUCTING EARTH

Author: [redacted]
Signature

Robert Anthony Charters
Name

[redacted]
Date